NAVAL POSTGRADUATE SCHOOL
Monterey, California

THESIS

ION DENSITY FLUCTUATIONS IN PLASMA AND THEIR EFFECTS ON HOT ELECTRON GENERATION

by

Marty Wallace
June 2002

Thesis Advisor: William L. Kruer
Second Reader: William B. Colson

Approved for public release; distribution is unlimited

THIS PAGE INTENTIONALLY LEFT BLANK

REPORT DOCUMENTATION PAGE			*Form Approved OMB No. 0704-0188*
Public reporting burden for this collection of information is estimated to average 1 hour per response, including the time for reviewing instruction, searching existing data sources, gathering and maintaining the data needed, and completing and reviewing the collection of information. Send comments regarding this burden estimate or any other aspect of this collection of information, including suggestions for reducing this burden, to Washington headquarters Services, Directorate for Information Operations and Reports, 1215 Jefferson Davis Highway, Suite 1204, Arlington, VA 22202-4302, and to the Office of Management and Budget, Paperwork Reduction Project (0704-0188) Washington DC 20503.			
1. AGENCY USE ONLY ***(Leave blank)***	**2. REPORT DATE** June 2002	**3. REPORT TYPE AND DATES COVERED** Master's Thesis	
4. TITLE AND SUBTITLE: **ION DENSITY FLUCTUATIONS IN PLASMA AND THEIR EFFECTS ON HOT ELECTRON GENERATION**			**5. FUNDING NUMBERS**
6. AUTHOR(S) Wallace, Martin C			
7. PERFORMING ORGANIZATION NAME(S) AND ADDRESS(ES) Naval Postgraduate School Monterey, CA 93943-5000			**8. PERFORMING ORGANIZATION REPORT NUMBER**
9. SPONSORING /MONITORING AGENCY NAME(S) AND ADDRESS(ES) N/A			**10.SPONSORING/MONITORING AGENCY REPORT NUMBER**
11. SUPPLEMENTARY NOTES The views expressed in this thesis are those of the author and do not reflect the official policy or position of the Department of Defense or the U.S. Government.			
12a. DISTRIBUTION / AVAILABILITY STATEMENT Approved for public release; distribution is unlimited			**12b.DISTRIBUTION CODE**

13. ABSTRACT ***(maximum 200 words)***

In this thesis, high-energy electron generation by stimulated Raman scattering of intense laser light is investigated in computer simulations. These high-energy electrons can be used to produce a high-energy x-ray source for Nuclear Weapons Effects Testing. The simulation results are compared with actual experiments conducted at the Atomic Weapons Establishment in the United Kingdom. The simulations show that the heated electron temperature is significantly lowered and the frequency spectrum of the scattered light is broadened by strong ion density fluctuations in the plasma. These density fluctuations are produced when the Raman scattered light undergoes Brillouin backscattering. Interactive Data Language is also used to analyze the spectrum of Raman scattered light in some recent experiments with the OMEGA laser at the University of Rochester.

14. SUBJECT TERMS Laser-plasma interactions, stimulated Raman scattering, plasma instabilities, ion density fluctuations			**15. NUMBER OF PAGES** 61
			16. PRICE CODE
17. SECURITY CLASSIFICATION OF REPORT Unclassified	**18. SECURITY CLASSIFICATION OF THIS PAGE** Unclassified	**19. SECURITY CLASSIFICATION OF ABSTRACT** Unclassified	**20. LIMITATION OF ABSTRACT** UL

NSN 7540-01-280-5500 Standard Form 298 (Rev. 2-89)
Prescribed by ANSI Std. 239-18

THIS PAGE INTENTIONALLY LEFT BLANK

Approved for public release; distribution is unlimited

ION DENSITY FLUCTUATIONS IN PLASMA AND THEIR EFFECTS ON HOT ELECTRON GENERATION

Martin C Wallace
Lieutenant, United States Navy
B.S., University of Washington, 1997

Submitted in partial fulfillment of the
requirements for the degree of

MASTER OF SCIENCE IN APPLIED PHYSICS

from the

NAVAL POSTGRADUATE SCHOOL
June 2002

Author: Martin C. Wallace

Approved by: William L. Kruer
Thesis Advisor

William B. Colson
Second Reader

William Maier II
Chairman, Department of Physics

THIS PAGE INTENTIONALLY LEFT BLANK

ABSTRACT

In this thesis, high-energy electron generation by stimulated Raman scattering of intense laser light is investigated in computer simulations. These high-energy electrons can be used to produce a high-energy x-ray source for Nuclear Weapons Effects Testing. The simulation results are compared with actual experiments conducted at the Atomic Weapons Establishment in the United Kingdom. The simulations show that the heated electron temperature is significantly lowered and the frequency spectrum of the scattered light is broadened by strong ion density fluctuations in the plasma. These density fluctuations are produced when the Raman scattered light undergoes Brillouin backscattering. Interactive Data Language is also used to analyze the spectrum of Raman scattered light in some recent experiments with the OMEGA laser at the University of Rochester.

THIS PAGE INTENTIONALLY LEFT BLANK

TABLE OF CONTENTS

THIS PAGE INTENTIONALLY LEFT BLANK

LIST OF FIGURES

THIS PAGE INTENTIONALLY LEFT BLANK

LIST OF SYMBOLS AND ACRONYMS

AWE	**Atomic Weapons Establishment**
c	**speed of light in a vacuum (3×10^8 m/s)**
e,q	**electron charge (1.602×10^{-19} C)**
E	**electric field (E_z denotes the electric field of the laser light wave, E_x denotes the electric field of the plasma wave)**
E_L	**electric field of laser**
FABS	**Full Aperature Backscatter System**
f_{HOT}	**fraction of laser energy absorbed into high-energy electrons**
I	**laser intensity (W/cm^2)**
IDL	**Interactive Data Language**
k	**wave number**
k_B	**Boltzmann's constant (1.38×10^{-23} J/K)**
k_{ia}	**ion acoustic wave number**
k_o	**wave number of incident laser light ($2\pi/\lambda$)**
k_{plasma}	**wave number of electron plasma wave**
k_s	**wave number of scattered light wave**
L	**length of PIC system**
LLNL	**Lawrence Livermore National Laboratories**
LLE	**Laboratory for Laser Energetics**
M	**mass of ions**
m_e	**electron mass (9.1×10^{-31} kg)**
n	**integer value used for calculating PIC parameters**
N_C	**number of cells within PIC system**
n_e	**plasma or electron density**
n_{cr}	**critical plasma density**
n_i	**density of ions**
NIF	**National Ignition Facility**
r	**radial distance from charge (wrt Debye length)**
SBS	**stimulated Brillouin scattering**
SRS	**stimulated Raman scattering**
T_e	**temperature (in keV) of electrons within plasma**
T_i	**temperature (in keV) of ions within plasma**
v	**velocity within PIC system**
v_{os}	**oscillation velocity of an electron in an electric field**
v_s	**ion acoustic velocity**
v_{th}	**electron thermal velocity (0.026 eV)**
x	**position within PIC system**
δ	**cell size or grid spacing for PIC code**
δ**E**	**perturbed electric field amplitude**
δ**n**	**density fluctuation**
δ**J**	**transverse current fluctuation**
δ**$P_{E\text{-field}}$**	**electric field pressure**
Δs	**increment of the charge density**

Δx	**displacement from i^{th} grid point**
ε_o	**permittivity constant (8.85×10^{-12} C/Nm^2)**
λ	**wavelength of light**
λ_D	**Debye length**
λ_o	**incident laser wavelength**
ω	**ion plasma frequency**
ϕ	**electrostatic potential of a charge at rest**
σ	**electron charge density**
ω	**angular frequency**
ω_{ek}	**Bohm-Gross corrected electron plasma frequency**
ω_{ia}	**ion acoustic frequency**
ω_o	**incident laser frequency**
ω_{pe}	**electron plasma frequency**

ACKNOWLEDGMENTS

- First of all, I would like to thank Dr. William L. Kruer, whom through his outstanding guidance and enthusiasm, motivated my interest in the field of plasma physics. His many hours spent driving down to the Naval Postgraduate School in Monterey from LLNL and talking with me about these plasma simulations are greatly appreciated.
- Second, I would like to thank Dan Gordon from NRL for his assistance in the analysis of the Turbowave program. He was able to take requested input from Dr. Kruer or myself and send us revised versions of Turbowave nearly instantaneously.
- Third, I would like to acknowledge Bob Kirkwood from Lawrence Livermore National Laboratories. He was my guide when I visited the OMEGA laser last summer and has been a great wall to bounce IDL analysis ideas off.
- Fourth, I would like to thank Major Mike Ortelli from DOE and Professor Chris Olsen from NPS for their assistance in the development of the IDL code that performs the experimental data analysis of SRS from OMEGA
- Finally, but foremost, I would like to thank my family for their support while I have been at NPS. My wife, Annie, has been very understanding of my long hours doing this research and has supported me to a fault throughout my career as a Naval Officer. My daughter, Emily, although only two, spent many long hours with me critiquing my thesis at home on the computer. I love them both very much.
- The plasma simulation capability at NPS and the collaborations with UCLA and LLNL were made possible by support from the Defense Threat Reduction Agency (DTRA) to investigate laser-plasma x-ray sources under NPS contract RPH4J.

THIS PAGE INTENTIONALLY LEFT BLANK

I. INTRODUCTION

In the Inertial Confinement Fusion (ICF) program, there has been a remarkable development of high power lasers, culminating in the National Ignition Facility now under construction at Lawrence Livermore National Laboratories. Such lasers are able to heat matter to very high temperatures and enable a great deal of high energy density physics to be explored in the laboratory. In this introduction, we will briefly discuss inertial confinement fusion and give an overview of this thesis work that considers another possible application of the National Ignition Facility (NIF). In the next two chapters, plasmas, plasma interactions, waves and instabilities, and plasma simulation will be discussed. In subsequent chapters, computer simulations of high-energy electron generation by intense laser light in underdense plasmas will be presented and discussed. Comparisons will then be made between our computer simulations and some real experimental data collected at the Atomic Weapons Establishment (AWE) and the Laboratory for Laser Energetics (LLE). Analysis of some measured scattered light spectra from the OMEGA laser at LLE will also be given.

THIS PAGE INTENTIONALLY LEFT BLANK

II. INERTIAL CONFINEMENT FUSION & NWET

Since the late 1940's the U.S. and other countries throughout the world have been searching for a means to replace our over reliance upon fossil fuels. Some of the methods currently being explored include solar voltaic cells, high efficiency wind power plants and wave energy converters that, in general, produce on the order of tens of kilowatts. An alternative path towards fossil fuel independence is inertial confinement fusion (ICF). This method, which can lead to power plants generating 1,000 megawatts of energy will be investigated using the National Ignition Facility located at Lawrence Livermore National Laboratories. Another important use for the NIF facility will be to conduct experiments to support the Stockpile Stewardship and Nuclear Weapons Effects Testing (NWET) programs. This thesis work is motivated by the potential use of NIF to generate a high-energy x-ray source for NWET.

There are currently two methods that are under consideration for inertial confinement fusion. The first approach, indirect drive, is characterized by directing the incoming laser beams onto a small cylinder constructed of some high Z material, such as gold. The surface of the cylinder starts to ablate; creating plasma that emits high-energy x-rays. The x-rays in turn drive the heating and compression of a deuterium-tritium target to fusion conditions. The second approach, direct drive, involves heating and compressing the fuel capsule by directly shining the laser beams onto the capsule. Each approach has advantages and disadvantages. Two major advantages of a direct drive method is the possibility of higher gain than an indirect-drive ICF and the ease at which a direct drive fusion power plant could be constructed in comparison with an indirect-drive power plant. On the other hand, indirect drive is less sensitive to non-uniformities in the laser beams and to the Raleigh-Taylor instability during the compression of the fuel capsule (Ref 1). The principal approach to ICF to be investigated with NIF will be indirect drive.

Another possible application for NIF is to produce a high-energy x-ray source for NWET, which motivates this thesis work. The x-rays would be produced by bremmstrahlung of high-energy electrons. The high-energy electrons are produced through the coupling of intense laser light that propagates through the underdense plasma. This non-linear phenomenon is known as stimulated Raman scattering (SRS).

In stimulated Raman scattering the laser light will decay into a scattered light wave plus an electron plasma wave. After a period of time, the plasma wave has increased in amplitude enough to accelerate electrons to a high velocity, making high-energy electrons. This process is most efficient when conducted with the density near 0.25 n_{cr}, where n_{cr} is the critical density. In theory, almost half of the laser light can then be transferred into high-energy electrons, an effect observed in early experiments using the 1.06 μm Shiva laser irradiating underdense plasmas within a hohlraum target. There is significant interest in researching the possibility of obtaining an efficient generation of high-energy electrons utilizing the National Ignition Facility. It is designed to operate at shorter wavelengths than Shiva (planned to be 0.35 μm and possibly 0.53 μm), but simulations have shown great promise in this area for NIF if the light is focused to sufficiently high intensity.

To explore this possibility, the hot electron generation by stimulated Raman scattering in plasma near 0.25 n_{cr} is investigated using computer simulations that utilize an electromagnetic, relativistic particle code. These computer simulations continue earlier thesis work by Major Mike Ortelli, USA and Captain David Jones, USA (Ref 2,3). Comparisons are made with experiments using 0.53 μm light at the Atomic Weapons Establishment (AWE) laboratory in the United Kingdom. About 50% absorption into hot electrons with an effective temperature of ~25 keV is found, in reasonable agreement with experimental results. The simulations show that the heated electron temperature has been significantly reduced and the frequency of the scattered light significantly broadened by the excitation of strong ion density fluctuations in the non-linear state. These fluctuations appear to be driven by the stimulated Brillouin scattering of the Raman scattered light (Ref 4,5).

Finally, stimulated Raman scattering is monitored in experiments by measuring the wavelength spectrum of the back-scattered light as a function of time. An example of such experimental data is analyzed using Interactive Data Language (IDL). The resulting spectrum can be used to monitor the density of the plasma and to show how the efficiency of the scattering varies with time.

III. PLASMA

Plasma is sometimes called the fourth state of matter. Although it makes up over 98% of the matter in the universe, in a strange quirk of physics it does not appear in a natural state on Earth. We utilize plasmas everyday, from the energy efficient fluorescent lights in your kitchen to the cathode ray tubes in older televisions. You can see it nearly daily in the Midwest in the form of lightning strikes, yet in practice it is usually only seen inside laboratories. Plasma is a quasi-neutral gas of charged and neutral particles that exhibits a collective behavior. The collective behavior comes from the fact that the plasma particles are charged. As these particles move around, they generate a local concentration of positive or negative charges, which gives rise to electric fields. The motions of the charges also induce magnetic fields. These fields affect the motion of charged particles far away. It is the long-ranged Coulomb force, which results from the solid angle volume of the affected plasma, which gives the plasma a myriad of possible interactions. (Ref 6)

A requirement that the Coulomb force of a neighboring particle be much less than the cumulative long range Coulomb force exerted by many distant particles will be satisfied when there are many particles in a Debye sphere. A Debye sphere is a sphere of radius one Debye length. A Debye length is a typical length over which a charged particle's bare electric field has significant influence. In terms of the density and temperature of the plasma components, the Debye length, l_D, can be defined by:

$$l_D = \left(\frac{e_o k_B T}{2 n_e e^2} \right)^{\frac{1}{2}} = 740 \left[\frac{T_{ev}}{n_e} \right]^{\frac{1}{2}} (cm)$$

where n, q and T are, respectively, the number density, charge and temperature of the particle species, either electrons or ions; k_B is Boltzmann's constant and e_o is the permittivity constant in vacuum.

For distances exceeding the Debye length the electric field of an individual charged particle is effectively shielded out by the surrounding plasma. If Φ is the electrostatic potential of a charge at rest in a plasma, then it can be shown that:

$$\Phi = \frac{q}{4 p e_o r} e^{-r / l_o}$$

where r is the radial distance from the charge. This potential differs from that of an isolated charge in a vacuum only by the exponential term. So, the Debye sphere, which is a sphere with radius equal to the Debye length, centered on the charge, is a charged particle's typical "sphere of influence" on neighboring plasma particles. Not surprisingly, the number of plasma particles that occupy this volume plays an important role in defining the Coulomb collisional properties of the plasma and determines the significance of discrete particle effects in general (Ref. 6).

When discussing plasmas it is common to refer to the temperature of the plasma in terms of energy due to the close relationship between the two properties. The average kinetic energy of a plasma is evaluated by 1/2 $\kappa_B T$ per degree of freedom, where k_B is the Boltzmann's constant and T is the plasma temperature in Kelvin. It is possible, and quite normal, to have several different temperatures within any given plasma. This is caused because electrons and ions have different temperatures, T_i and T_e and thus their Maxwellian distributions are different. If there were a magnetic field applied, two different temperatures within the same species can occur, since forces act differently about the parallel and perpendicular axis. Typical plasma may have temperatures on the order of a million Kelvin or approximately 100 eV.

1 eV = 11,600 K

A. PLASMA INTERACTIONS

The fact that plasma particles behave collectively means that plasmas can support a wide variety of wave motions and oscillations. One such basic oscillation arises if a group of electrons is slightly displaced from their equilibrium positions. The displaced electrons feel an electrostatic force seeking to return them to their equilibrium positions, but upon arrival there they now have a kinetic energy equal to the potential energy of their initial displacement. The electrons overshoot, reconvert their kinetic energy to potential energy and a simple oscillation is set up. The frequency of this fundamental oscillation is known as the plasma frequency, w_{pe} and is defined by:

$$w_{pe}^2 = \frac{n_e e^2}{e_o m_e}$$

where n_e is the mean plasma density and m_e is the electron mass. (Ref. 6) The oscillation is of such a time scale that the ions do not have an opportunity to react to the oscillating field and they are assumed to be fixed. The equation above is derived with the following assumptions: 1) there is no magnetic field, 2) there are no thermal motions ($\kappa_B T=0$), 3) the ions are fixed in space in a uniform distribution, 4) the plasma is infinite in extent and 5) the electron motions occur only in one direction. This plasma oscillation can most properly be described as a plasma wave, because the fringing electric field causes a coupling of the disturbance to adjacent layers, and the oscillation does not stay localized. Additionally, when electrons stream into adjacent layers within a plasma, their thermal velocities will bring information about what is happening in the oscillating region of the plasma.

The angular frequency and the wave vector are functionally related to one another, at least in linear theories of plasma waves, by a dispersion relationship. Knowledge of the dispersion characteristics of the propagating waves is certainly necessary for an understanding of the plasma state. In a simple one-dimensional problem the dispersion relationship is as follows:

$$w^2 = w_{pe}^2 + \frac{3}{2}k^2 u_{th}^2$$

where w is the wave frequency, k is the wave number, w_{pe} is the plasma frequency and the thermal velocity is defined by, $v_{th}^2 = 2k_B T_e / m_e$. This additional thermal correction is known as the Bohm-Gross correction. The frequency is now dependent on k and the group velocity is finite. There is an imaginary component from the derivation of the equation above which results in a linear damping term known as Landau damping.

Landau damping is a physical effect that is related to the details of the underlying velocity distribution functions of the plasma particles. It occurs in the absence of short-range binary collisions and hence it is sometimes called collision-less damping. In plasma, an initial disturbance is damped (in the absence of binary Coulomb collisions) as it propagates away from its point of origin. This can be explained by the following argument. Those particles that interact most strongly with a plasma wave are those whose velocities are closest to the wave phase velocity. These particles see an approximately

stationary electric field. In a stable thermal distribution, for any particular wave speed, there are always more particles traveling slightly slower than the wave than those traveling slightly faster than the wave. If the particles traveling slower than the wave are accelerated by the wave and take energy from it, and those that travel faster than the wave give energy to the wave, then there are more particles taking energy from the wave than those giving energy to it and the wave damps. Electrons that approach the phase velocity of the plasma wave will take energy out the wave and thus gain momentum (Ref 4).

With our basic background in some of the definitive properties of plasma, we can now investigate how electromagnetic waves in the form of a laser light interact with plasma and create the instability cycle which perpetuates the increase in the magnitude of the plasma wave through Raman scattering.

B. PLASMA INSTABILITIES

First of all though, we should look at frequency and wave number matching conditions required for Raman scattering to occur. Raman scattering can be seen as simply the resonant decay of an incident photon into a scattered photon plus an electron plasma wave (or plasmon). The frequency and wave number matching conditions then become:

$$w_o = w_s + w_{ek}$$

$$k_o = k_s + k_{plasma}$$

where w_o and k_o are the frequency and wave number for the incident light wave, w_s and k_s are for the scattered light wave, while w_{ek} and k_{plasma} are for the electron plasma wave. It is clear that the minimum frequency of light within the plasma must be at least ω_{pe}, therefore $\omega_o \geq 2\omega_{pe}$. Light will not propagate if $\omega_{pe} > \omega$. Because $n_e/n_{cr} = (\omega_{pe}/\omega_0)^2$, then $n_e \leq 0.25 n_{cr}$, where n_e is the plasma density and n_{cr} is the critical density (Ref. 4). The fraction of energy that is deposited in the plasma wave heats the plasma as the wave damps. This kinetic energy increase is what produces the high-energy electrons that are characteristic of the Raman instability. However, since these electrons can preheat the fuel in laser fusion applications, this instability has to be monitored carefully.

The Raman instability provides a mechanism by which the electron plasma wave and the associated scattered wave can build up in amplitude utilizing a feedback system. Figure 1 shows the stages of the instability cycle.

During the first stage any perturbation, such as thermal noise can cause a small charge density fluctuation to occur. This density fluctuation, dn, is due to a thermal level plasma oscillation. The oscillatory motion of electrons in the light couples with dn to induce a transverse current fluctuation:

$$dJ = \frac{-e^2 E_L dn}{m_e w_o}$$

where e is the electron charge, E_L is the laser electric field, $m_e$is the mass of an electron and w_o is the light wave frequency.

The perturbed current produced, dJ, will then drive the scattered light wave at the beat frequency. The scattered light wave grows from noise as a perturbed wave with electric field amplitude, dE (a light wave at an up shifted or downshifted frequency). Finally this electric field will beat in turn with the electric field produced by the laser to create a perturbation in the electric field pressure.

$$dP_{E-field} = \frac{e_o}{2}(E_L + dE)^2 - \frac{e_o}{2}E_L^2 = e_o E_L dE$$

This pressure perturbation will then reinforce the initial density fluctuation. This feedback system leads to exponential growth of both the plasma wave (δn) and the scattered light wave (δE) (Refs. 4,7,8,9).

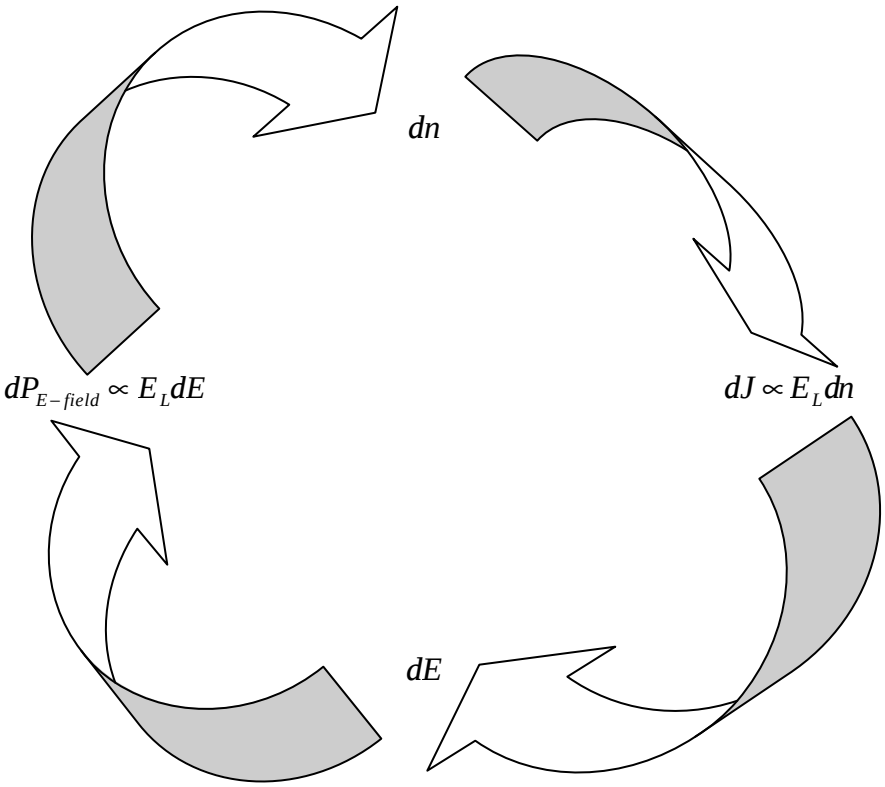

Figure 1. Plasma instability feedback loop for Raman backscatter growing from noise.

A second important instability is stimulated Brillouin scattering, which involves the production of a scattered light wave plus a low frequency ion acoustic wave. The production of the ion acoustic wave is similar in manner to the production of the Raman instability, except that resonant decay of the incident photon results in a scattered photon plus an ion acoustic phonon. The frequency and wave number matching then becomes:

$$w_o = w_s + w_{ia}$$

$$k_o = k_s + k_{ia}$$

where w_{ia} and k_{ia} are for the ion acoustic wave. The frequency of the ion acoustic wave is much less than either the plasma frequency or the incident photon frequency. Therefore this instability can exist at all densities up to the critical density. Brillouin scattering is a significant concern in laser fusion research, because nearly all of the energy can be transferred to the scattered light wave. This may appreciably degrade the rate of absorption, and SBS can also lead to deep density modulations in the plasmas that will be

discussed later. If the wavelength of the ion acoustic waves is considered to be small by taking $k^2 l_D^2 >> 1$, then the dispersion relationship becomes:

$$w^2 = \frac{n_o e^2}{e_o M}$$

where M is the ion mass. There becomes a complementary behavior between the ion acoustic waves and the electron plasma wave. At higher wave numbers the ion acoustic waves exhibit a constant frequency, but become constant velocity at smaller k values. The electron plasma waves are constant velocity at high k values, but become constant frequency at small k values (Ref 4,5,6). This is shown graphically in Figure 2, where v_{th} is the thermal velocity, v_s is the ion acoustic velocity and Ω_p represents the ion plasma frequency.

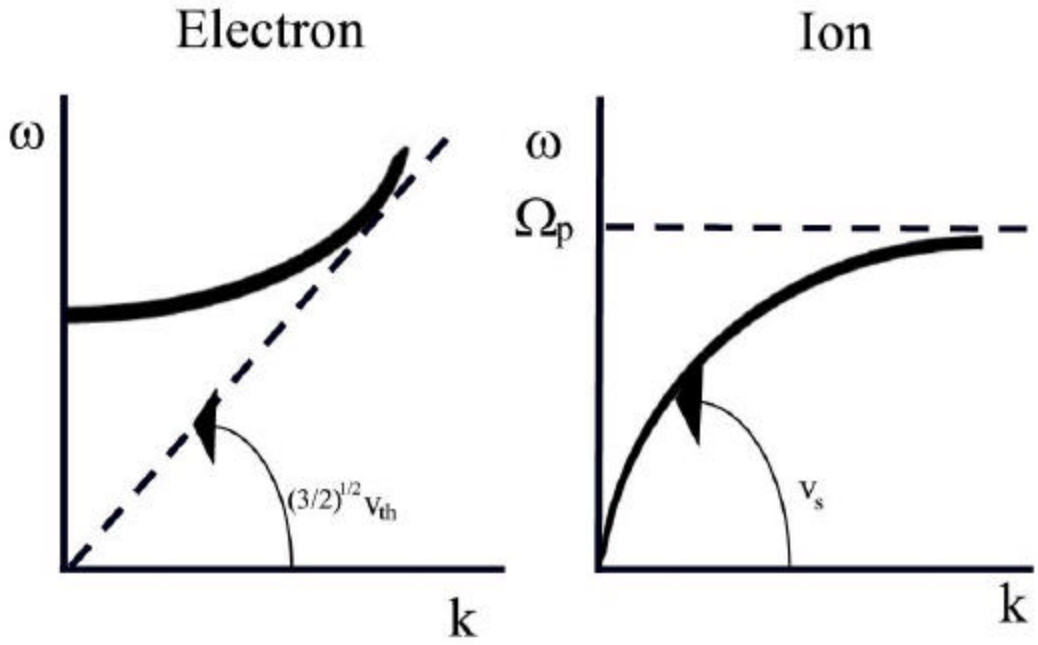

Figure 2. Comparison of the dispersion curves for electron plasma and ion acoustic waves

THIS PAGE INTENTIONALLY LEFT BLANK

IV. GREEN LIGHT COMPUTER SIMULATIONS

The advancement in the past three decades in laser power output and computer-processing speed has played a critical part in the ability to analyze laser-plasma interactions. As an example, the development of the SHIVA laser by Lawrence Livermore National Laboratories (LLNL) in 1978 was one of the first steps in creating a mega-joule class laser. SHIVA was rated at 10 kilojoules and was superceded by the NOVA laser, which was rated at 40+ kilojoules, in 1984. Today construction continues on the NIF laser at LLNL, which will be used for laser fusion research and stockpile stewardship. NIF is expected to be fully operational by 2008 and will have a 1.8 mega-joule output of 0.35 μm light. This means that on a rough average, the laser capacity output of some of the largest lasers in the world doubles about every three years. Similar in comparison is the progression of computer processing. Gordon Moore, co-founder of Intel, made an observation in 1965 that the number of transistors per square inch on integrated circuits had doubled every year since the integrated circuit was invented. Moore predicted that this trend would continue for the foreseeable future. In subsequent years, the pace slowed down, but data density has doubled approximately every 18 months. This is the current definition of Moore's Law. Most experts expect Moore's Law to hold for at least another two decades.

Computer simulations have become an extremely important facet in the analysis of laser plasma interactions. In the early years of computer simulation of plasmas, the "supercomputers" at the time could only handle on the order of a thousand or so particles. These room-sized computers could only manipulate the most rudimentary calculations and took a great deal of time to do so. Today, an ordinary laptop or desktop computer with a sizeable amount of memory can easily handle hundreds of thousands of particles and larger mainframes can handle very complex multi-dimensional problems with millions of particles.

The Department of Energy (DOE) is currently utilizing ASCI White, a IBM constructed computer at LLNL capable of calculating 12.3 trillion floating point operations per second (Teraflops), to simulate nuclear weapons testing. These simulations are essential due to the U.S. observation of the Comprehensive Test Ban Treaty. Without the possibility of conducting underground tests, the computer simulations help make sure that the nuclear weapons stockpile is safe, reliable and operational. With ASCI White, we can analyze the factors involved in a nuclear detonation. In 2004, there will be a 60 Teraflops supercomputer known as ASCI Purple at LLNL. The current ASCI project is expected to have a 100 Teraflops supercomputer by about 2006. As a comparison of the progress in computing power, in 1985 it would have taken the fastest supercomputer 60,000 years to perform the full three-dimensional nuclear simulation that this future supercomputer will be able to accomplish in less than a month!

A. Particle in Cell Code Simulations

Computer simulations using Particle in Cell (PIC) codes offers scientists a powerful and direct approach in the investigation of kinetic and non-linear effects. An example of the basic cycle of the PIC code is shown in Figure 3.

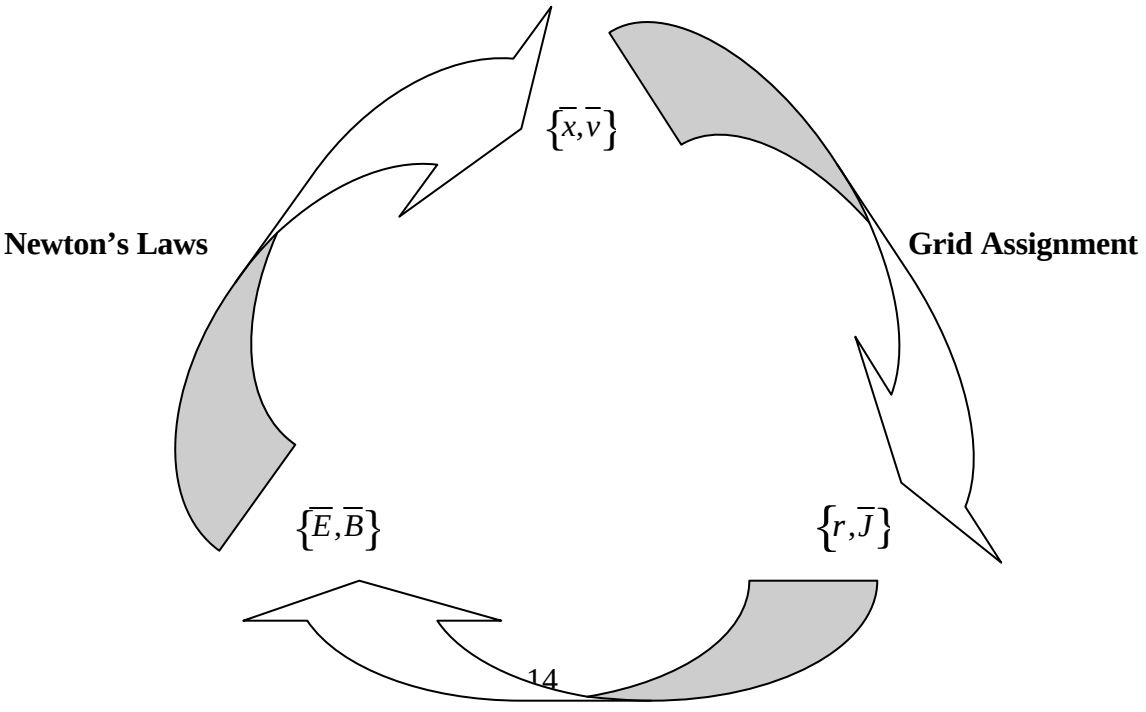

Maxwell's Equations

Figure 3. Particle code simulation cycle.

It would be constructive to cover the components of a very basic PIC code. For simplicity, we treat ions as a fixed and neutral background in this introductory discussion. We can sometimes make this assumption because the mass of the ions is so much larger than that of the electrons. Secondly, we impose no magnetic fields. In the limit of electrostatics, the magnetic field generated by plasma currents is negligible. Hence, we only consider electrostatic fields and Maxwell's equations reduce to $e_o \vec{\nabla} \bullet \vec{E} = s$, where s is the charge density. In the interest of producing a very simple code, variations are allowed only in one direction. The problem starts off by calculating the charge density. This is accomplished by dividing the system created into a number of cells that are determined by the user in the computer code. The cell size, d, is then made unity which allows $L = N_C$, where L is the length of the system and N_C is the number of cells within the system. Periodic boundary conditions will be used in this simplest example, meaning that charges leaving the system on the left (right) boundary are simply reintroduced on the right (left) boundary. The charge can simply be assigned to its nearest grid point location; however it is better to share the charge between its two nearest grid points (Figure 4). For a charge located a distance Δx to the right of the i^{th} grid point, you have:

$$\Delta s\,(i) = q(1-\Delta x)$$

$$\Delta s\,(i+1) = q\Delta x$$

where q is the basic electron charge and Δs is the increment in the charge density. Once the charge is assigned on the spatial grid, the electric field is determined next using Poisson's equation in the one-dimensional form.

$$e_o \frac{\P E}{\P x} = -e(n_i - n_e)$$

where n_i is the ion density and n_e is the electron density.

One possible method is to Fourier transform the charge density and Poisson's equation. The inversion of the Fourier transform will give the electric field on the spatial grid. An easier method is to use finite differences.

$$E(i+1) = E(i) + 4pd\left[\frac{s(i+1) + s(i)}{2}\right]$$

The electrical force is assigned to each of the particles using the same method used to assign the charge to the grid. By considering a particle a distance Δx to right of the i^{th} grid point, the force F on the particle is determined by linear interpolation.

$$F = qE(i)[1-\Delta x] + qE(i+1)\Delta x$$

The velocity, v, and position, x, of each particle are then advanced Δt in time using a "leap frog" algorithm.

$$v^{n+\frac{1}{2}} = v^{n-\frac{1}{2}} + F^n \Delta t$$

$$x^{n+1} = x^n + v^{n+\frac{1}{2}} \Delta t$$

Each of the superscripts denotes a time step. If x and v are defined as being one-half time step apart, then second order accuracy is achieved. Initially, position and velocity can be defined at the same time, but the velocity can be displaced backwards using the force at t=0.

The plasma cycle continues to be computed by using a time step small enough to resolve the characteristic oscillations of the plasma, usually the electron plasma frequency. The time step commonly used is on the order of $0.2\omega_{pe}$. A grid size of about λ_{DE} helps resolve the scale lengths characteristic of the collective behavior. Aliasing is a numerical instability that arises when the wave number k cannot be distinguished from spurious ones with wave numbers $k + (2pn/d)$, where d is the grid spacing and n is an integer. This can be eliminated by not choosing the grid size to be a small fraction of the Debye length (Ref 10).

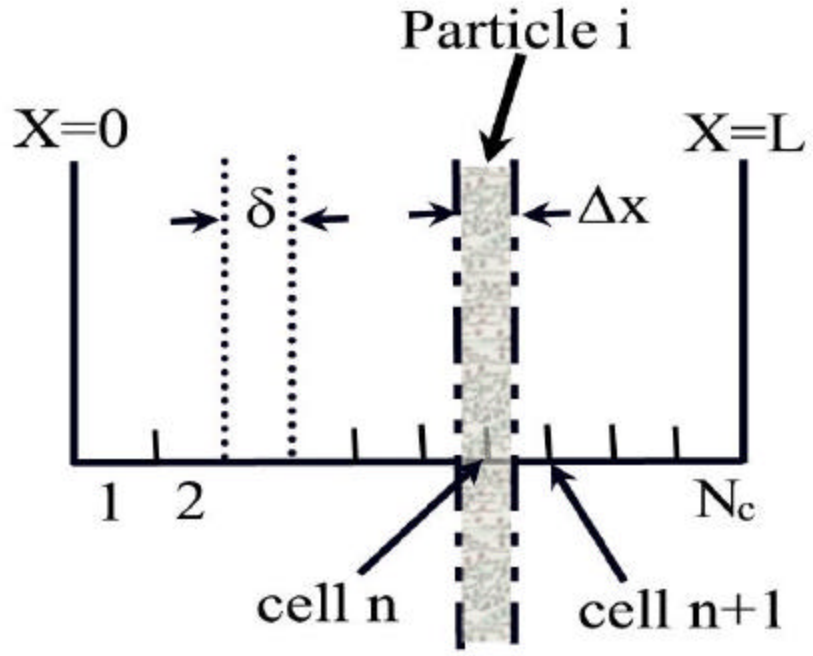

Figure 4. Particle in cell code sharing method

B. TURBOWAVE AND THE AWE EXPERIMENTAL ANALYSIS

One of the possible uses for the National Ignition Facility (NIF) is to generate high-energy electrons with an effective temperature of between 20-50 keV using either 0.53μm or 0.35μm laser light in order to produce a high-energy x-ray source for nuclear weapons effects testing. Computer simulations are used to investigate generation of these high-energy electrons via stimulated Raman scattering (SRS) of intense laser light (Ref 8,9). It is shown that a fairly efficient hot electron generation (~50%) can be achieved if plasma with a density near 0.25 n_{cr} is irradiated with sufficiently intense laser light. The calculations compare favorably with the hot electron generation observed in recent Atomic Weapons Establishment (AWE) experiments in the United Kingdom using intense 0.53 μm light. Similar results are theoretically expected for 0.35 μm light

provided that the plasma density and laser intensity are scaled about a factor of two higher.

The computer simulations are carried out using Turbowave, a parallel 3-D, electromagnetic, relativistic particle code written by Dan Gordon from the Naval Research Laboratory (NRL). In contrast to the simple case discussed to illustrate the concepts, this particle in cell (PIC) code solves Maxwell's equations along with the relativistic equations of motion of many electrons and ions, which represent the plasma. One and two-dimensional simulations were used to follow the propagation of intense laser light through a slab of plasma, as indicated in Figure 5. Periodic boundary conditions are used in the other directions. Particles striking the left or right boundaries are re-emitted with their original thermal distribution. The laser light is sent in from the left boundary, and light waves striking the left or right boundaries are allowed to pass out of the system (Ref 11).

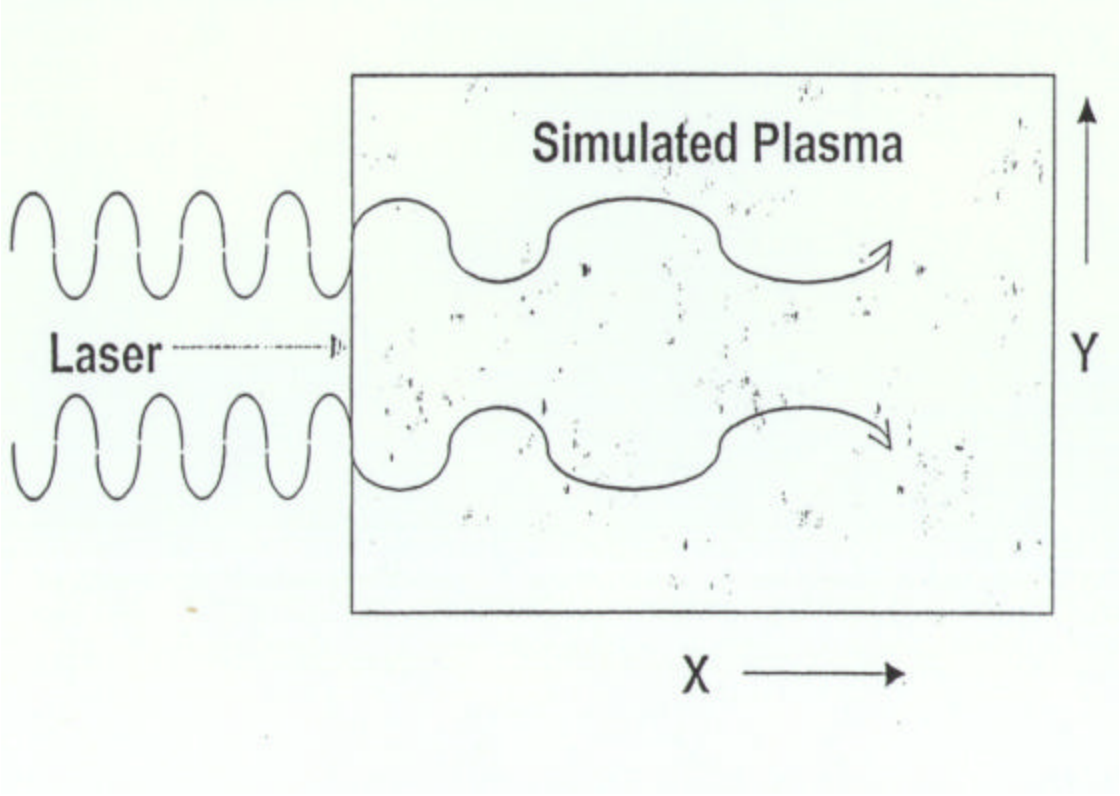

Figure 5. Intense laser light interactions with plasma slab

1. Atomic Weapons Establishment HELEN Experiments

Many simulations have been carried out with a wide variance in plasma densities, laser intensities, and electron and ion temperatures. We will discuss an instructive 1-D simulation that was motivated by the recent experiments at AWE. For this simulation, the initial uniform plasma density is 0.23 n_{cr}, where n_{cr} is the density at which the incident light striking the plasma is totally reflected. We are choosing a uniform, collisionless plasma with density $w_{pe}/w_o = 1/2.1 = \sqrt{n_e/n_{cr}}$. The following other parameters are also considered:

- The electron temperature, T_e, is 2.5 keV, the ion temperature, T_i is 0.625 keV,
- The size of the uniform plasma slab is 68.5 free space wavelengths for the laser light or a plasma length of $204.8c/w_{pe}$
- $v_{os}/c = 0.04$ (the driver's amplitude, related to the dimensionless laser intensity; υ_{os} is the electron's velocity as a result of the laser's electric field)
- Duration of the run is $3277/w_{pe}$ or 1.94 x 10^{-12} seconds, which is sufficient for the rapidly growing instability to saturate.

As the laser light propagates through the plasma slab, it undergoes stimulated Raman scattering, i.e., it decays into a backscattered light wave plus an electron plasma wave with a frequency that is principally ω_{pe}, the electron plasma frequency, plus a small thermal correction. Due to the instability discussed earlier, the electron plasma wave and the scattered light wave will continue to grow in amplitude. The fraction of energy that is deposited into the wave is responsible for the increase in kinetic energy that results in the production of hot electrons.

The efficiency of the electron heating can be obtained by monitoring the various energy histories in the simulation. Figure 6 shows the evolution of the kinetic energy of

the plasma, the energy carried off when the heated particles exit the boundaries, the energy in the electric and magnetic fields in the plasma, as well as the Poynting flux through the left and right boundaries. At the end of the run, the kinetic energy is about 0.4 (dimensionless units used), which is up from about 0.15 initially. The lost particle energy equates to about 0.3. If these energies are added together and divided by the total energy input (the amount of energy crossing the right boundary as if there were no plasma present) from the laser, you obtain an estimated absorption. The energy output from the right boundary is about 1.15; therefore, the fraction of the incident laser energy absorbed is about 48.7%.

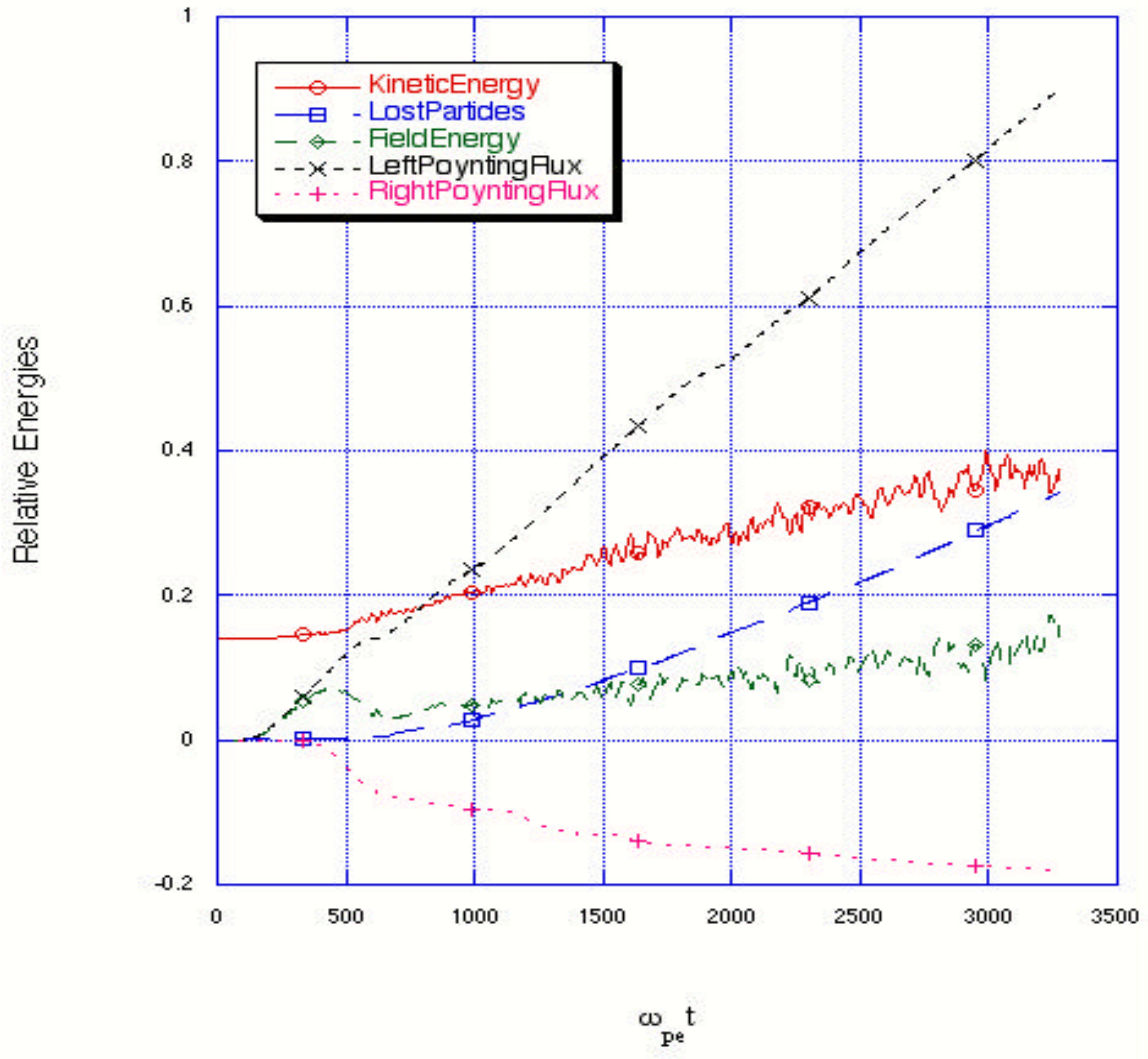

Figure 6. Energy diagram for 2.5 keV computer simulations.

For this simulation, about 50% of the incident laser energy is absorbed into heated electrons. This compares reasonably well with the analogous experiment, where about 20% absorption into high-energy electrons was measured. These experiments with the HELEN laser in the United Kingdom at AWE were conducted utilizing various average plasma densities and laser intensities irradiated with a single 2ω unsmoothed beam (Ref. 10). Figure 7 shows the fraction of the laser energy absorbed into high-energy electrons (f_{HOT}) as a function of average plasma density. It can be seen that f_{HOT} is a function of both plasma density and laser intensity, with a peak being centered at about 0.25 n_{cr} where the maximum amount of absorption takes place. Of course, there is actually a range of densities in the experiment, so some absorption into hot electrons occurs even when the average density exceeds 0.25 n_{cr}, the maximum density for which SRS occurs.

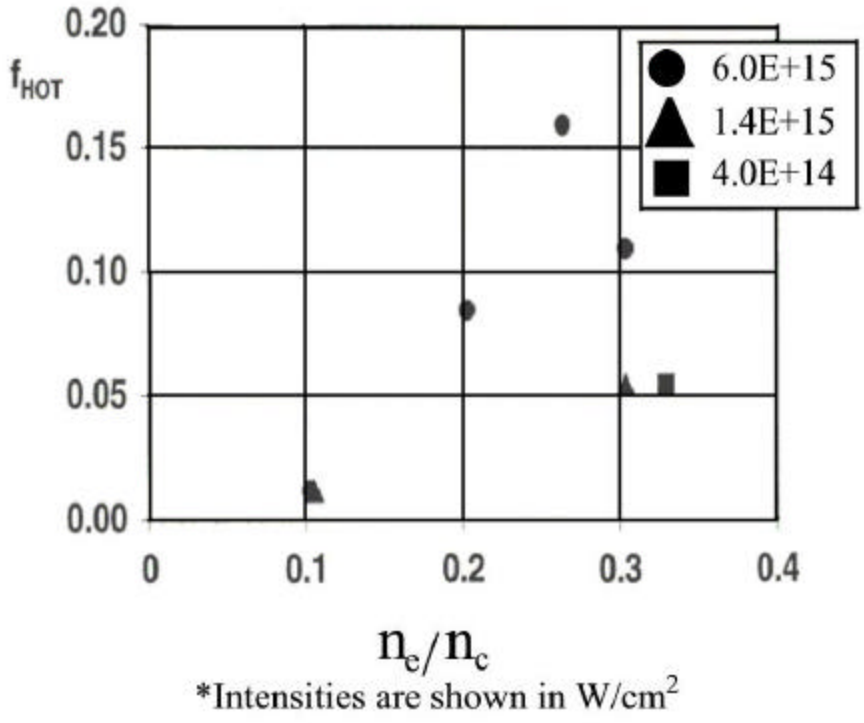

Figure 7. High f_{HOT} only with high intensity, unsmoothed beams

The lesser absorption is to be expected as the laser beam had to first form the plasma in this particular experiment. We estimate that the ideal conditions for SRS were only obtained during the second half of the laser pulse. In addition, the intensity of the laser light was somewhat less in the experiment. The equation for intensity for this simulation is:

$$I = \frac{1.35x10^{18}a^2}{l_m^2} = \frac{1.35x10^{18}(0.04)^2}{(0.532)^2} = 7.63x10^{15}\text{W/cm}^2$$

where $a = v_{os}/c$.

When the electric field of the plasma wave becomes sufficiently large, electrons are accelerated to high energies, producing a high-energy tail on the electron energy distribution. An example of this high-energy tail is shown in Figures 8a and 8b. In the plots you can see the probability distribution of electrons plotted, as a function of energy expressed as a percentage of the rest mass energy. The slope of the distribution gives the heated electron temperature. For comparison, we look at the high-energy tail without ion motion not allowed (essentially making the ions of infinite mass). In Figure 8a, the effect of ion motion not being allowed is quite apparent. The hot electron temperature, determined from the slope of the distribution at high energy is almost 130 keV!

In a more realistic scenario, however, we must include ion motion and allow ion density fluctuations to develop. Figure 8b shows the results when ions are allowed to move. In this case, the hot electron temperature is about 26 keV. This means an overall reduction in the hot electron temperature of almost 80%, showing that the ion density fluctuations created severely reduce the characteristic temperature of the high-energy electrons.

The hot electron temperature compares very favorably with actual data obtained from testing at AWE. The measured T_{hot} during HELEN experiments was approximately 30 keV. It is important to note that this heated electron temperature has been

significantly reduced by the development of pronounced ion density fluctuations in the plasma.

Figure 8a. High energy tail distribution with no ion motion (~130 keV)

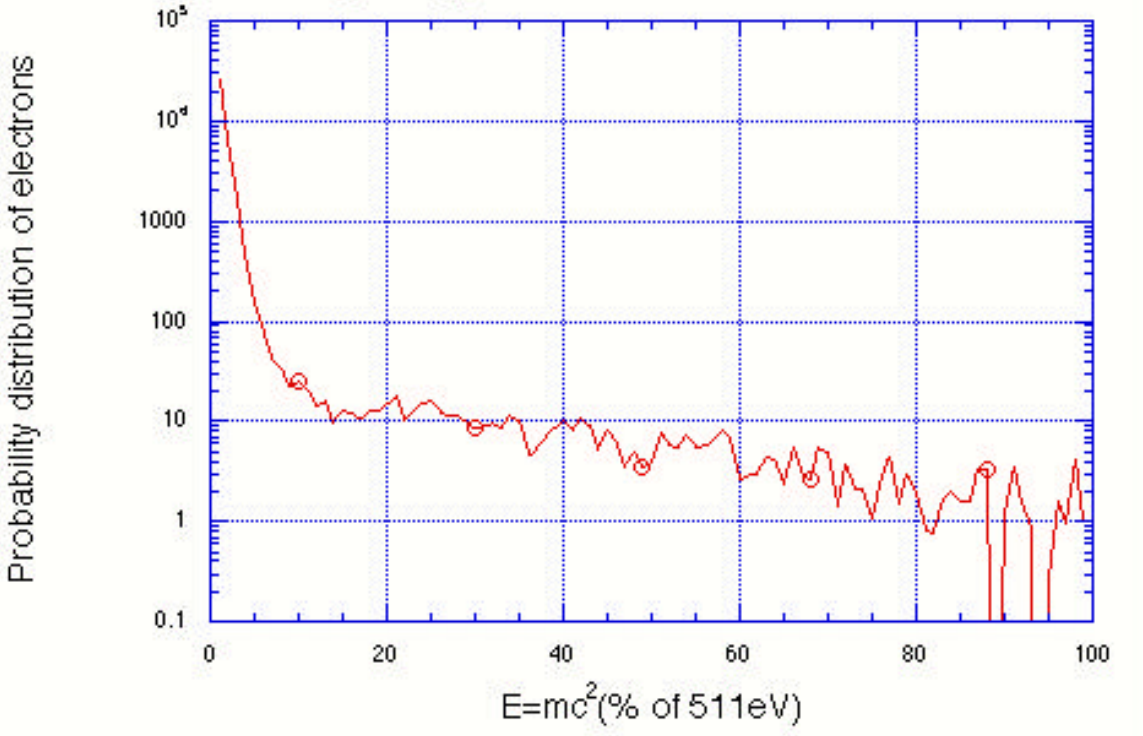

Figure 8b. High energy tail distribution with ion motion allowed (~26 keV)

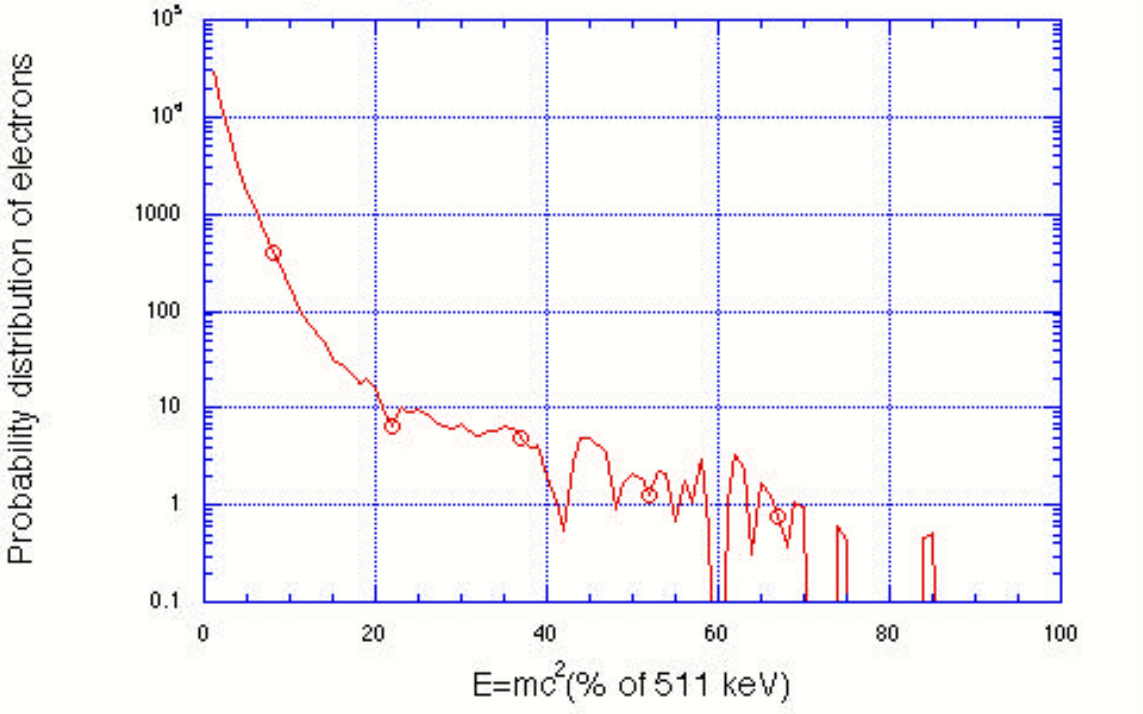

Figure 8. Hot electron energy distribution for 2.5 keV computer simulation

The evolution of the plasma density fluctuations is shown in Figures 9 and 10. Figure 9a shows the simulation early on when the density fluctuations have not yet developed. In Figure 9b, you can see the ion density fluctuations beginning to propagate within the first half of the plasma. Figure 10a shows the initial development of deeply modulated ion fluctuations. Finally 10b, on a slightly different scale to emphasize the deep canyons in the density, shows the final evolution of the plasma modulations.

The fluctuations reduce the heated temperature since they couple the Raman-generated plasma waves into plasma waves with a slower phase velocity, which in turn accelerate electrons to lower energies. These ion density fluctuations have a rather long wavelength (about three times λ_o, the incident laser wavelength). The fluctuations have a simply physical explanation. In the near 0.25 n_{cr} plasma, the Raman scattered light wave has a frequency near ω_{pe} and a long wavelength (about $6\lambda_o$). This scattered light wave becomes large in amplitude and undergoes simulated Brillouin scattering (SBS), which corresponds to its decay into a backscattered light wave plus an ion acoustic wave. The ion density fluctuations associated with this ion acoustic wave have a wavelength of about $3\lambda_o$, in agreement with the results in Figure 10b.

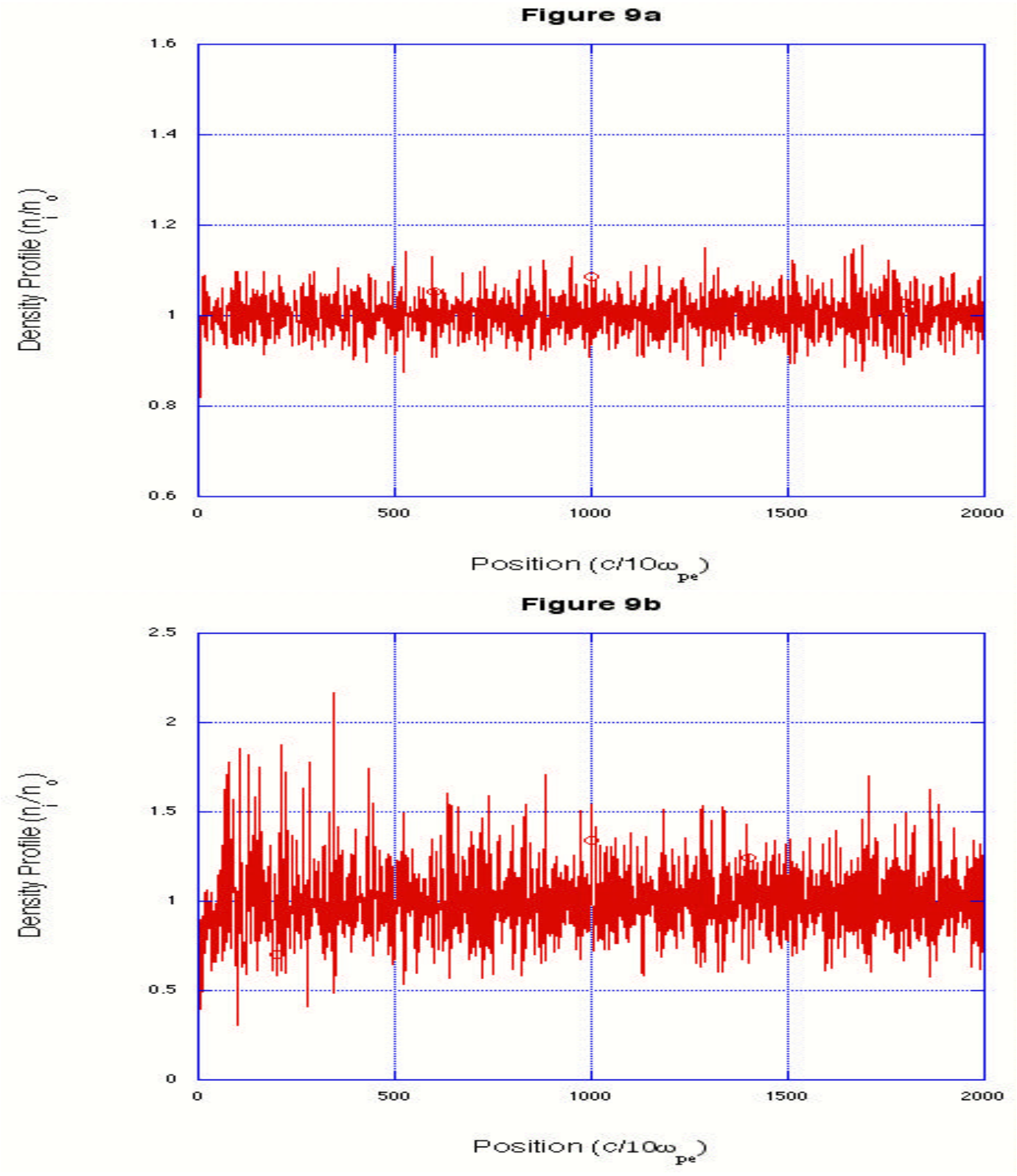

Figure 9. Plasma density fluctuations for 2.5 keV plasma run (early)

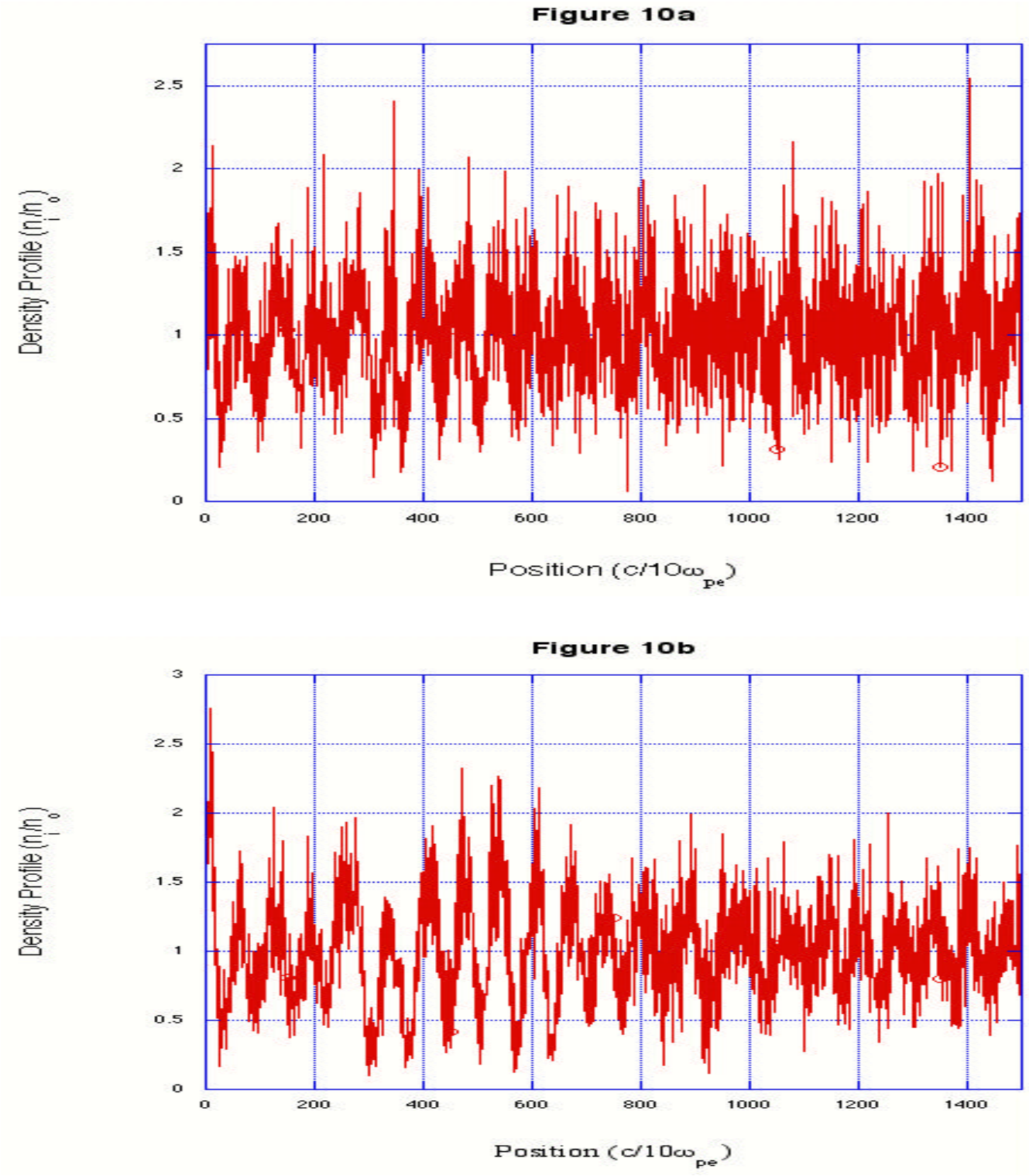

Figure 10. Plasma density fluctuations for 2.5 keV plasma run (late)

Let's now consider a simulation with a lower electron temperature, as this may be closer to actual experimental temperatures. For this simulation, the initial uniform plasma density is again 0.23 n_{cr}, where n_{cr} is the density at which all incident light striking the plasma is totally reflected. We are choosing a uniform, collisionless plasma with density $w_{pe}/w_o = 1/2.1 = \sqrt{n_e/n_{cr}}$. The following other parameters are also considered:

- The electron temperature, T_e, is 1 keV, the ion temperature, T_i is 0.25 keV,
- The size of the uniform plasma slab is 68.5 free space wavelengths for the laser light or a plasma length of $204.8c/w_{pe}$,
- $v_{os}/c = 0.04$ (the driver's amplitude, related to the dimensionless laser intensity; υ_{os} is the electron's velocity as a result of the laser's electric field),
- Duration of the run is $3277/w_{pe}$ or 1.94 x 10^{-12} seconds.

With a reduced background electron temperature we find that the amount of Raman scattering and the high-energy electron temperature are about the same as before. We use the same data analysis as for the earlier computer simulation. The efficiency of the electron heating is obtained by analyzing the energy diagram for the 1 keV simulation. Figure 10 shows the evolution of the kinetic energy of the plasma, the energy carried off when the heated particles exit the boundaries, the energy in the electric and magnetic fields in the plasma, as well as the Poynting flux through the left and right boundaries. At the end of the run, the kinetic energy is about 0.24 (dimensionless units used), which is up from about 0.04 initially. The lost particle energy equates to about 0.24. If these energies are added together and divided by the total energy input (the amount of energy crossing the right boundary as if there were no plasma present) from the laser, you obtain the total absorption. The energy output from the right boundary is about 1.0, therefore the amount of laser light absorption is about 44.0%, about the same as in the previous example.

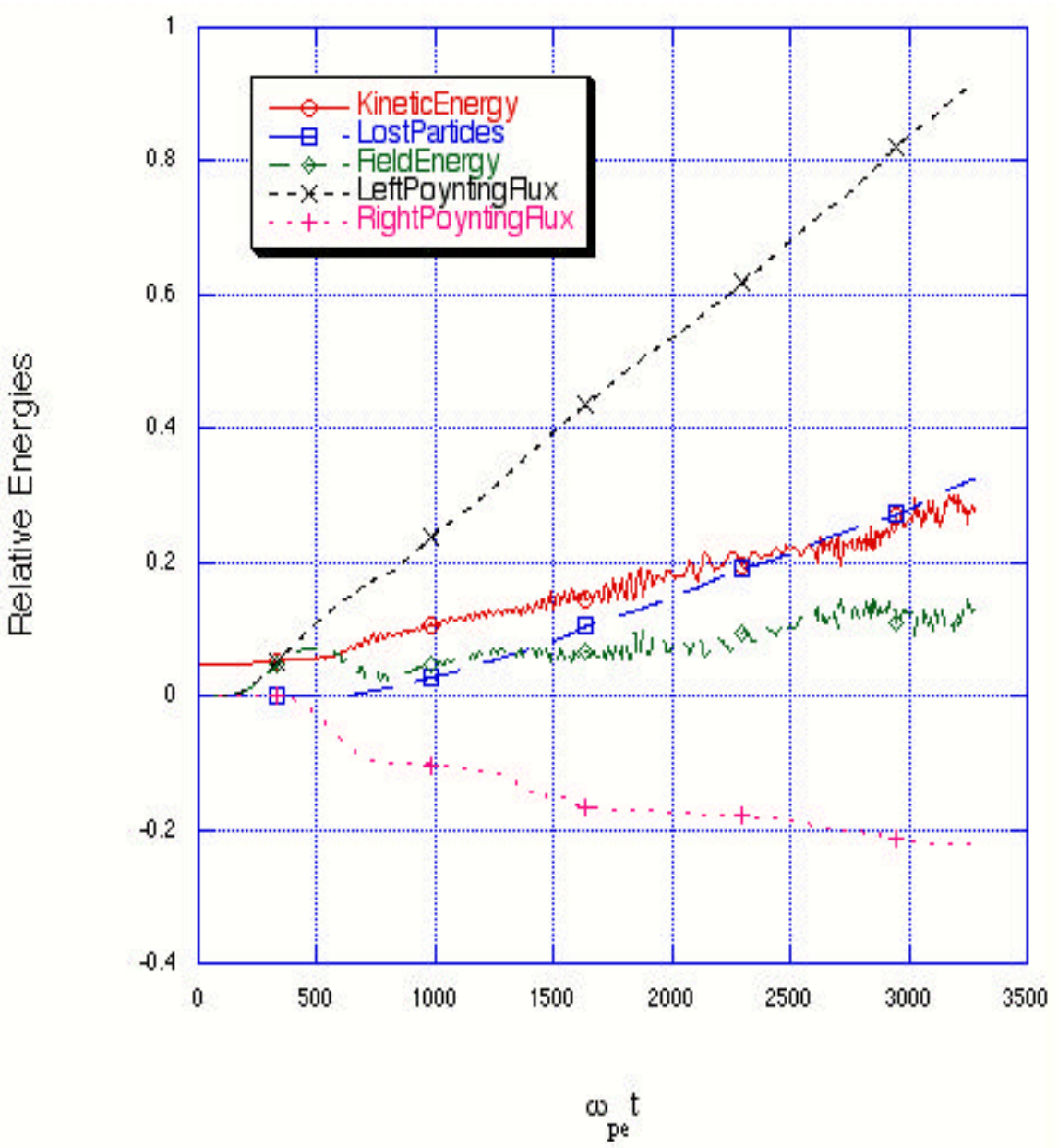

Figure 11. Energy diagram for 1 keV computer simulation.

Next we examine the high-energy tail created by the Raman instability. We notice that the average temperature of the hot electrons is similar to the 2.5 keV simulation. Figure 12 shows the heated electron distribution function. From the slope, the heated electron temperature can again be found. For this 1keV input, you receive an average electron temperature of 20.4 keV, a bit lower than before.

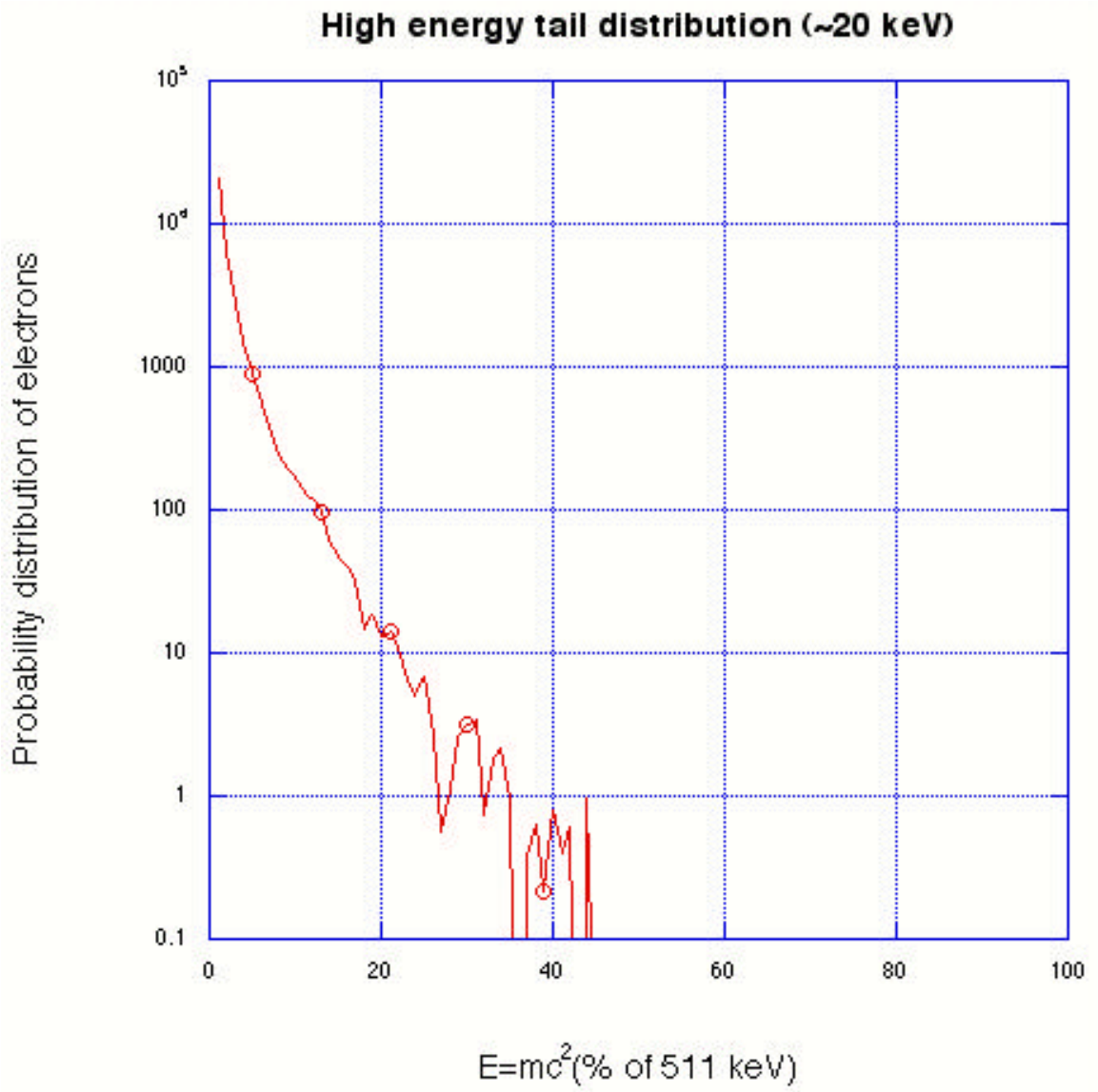

Figure 12. Hot electron energy distribution for 1 keV computer simulation

Displays of the plasma fluctuations for the 1 keV simulation are shown in Figures 13 and 14. Figure 13a shows the timeframe in which the plasma fluctuations have not yet developed. In Figure 13b, you see the magnitude of the ion density fluctuations starting to increase strongly, on a relative scale. Figure 14a shows the development of the modulated fluctuations throughout the plasma, somewhat different from the 2.5 keV case in which the fluctuations were only deeply modulated in the first half of the plasma. Finally Figure 14b shows that the deep modulations are occurring throughout the entire length of the plasma. The fluctuations reduce the heated temperature since they couple the Raman-generated plasma waves into plasma waves with a slower phase velocity, which in turn accelerate electrons to lower energies.

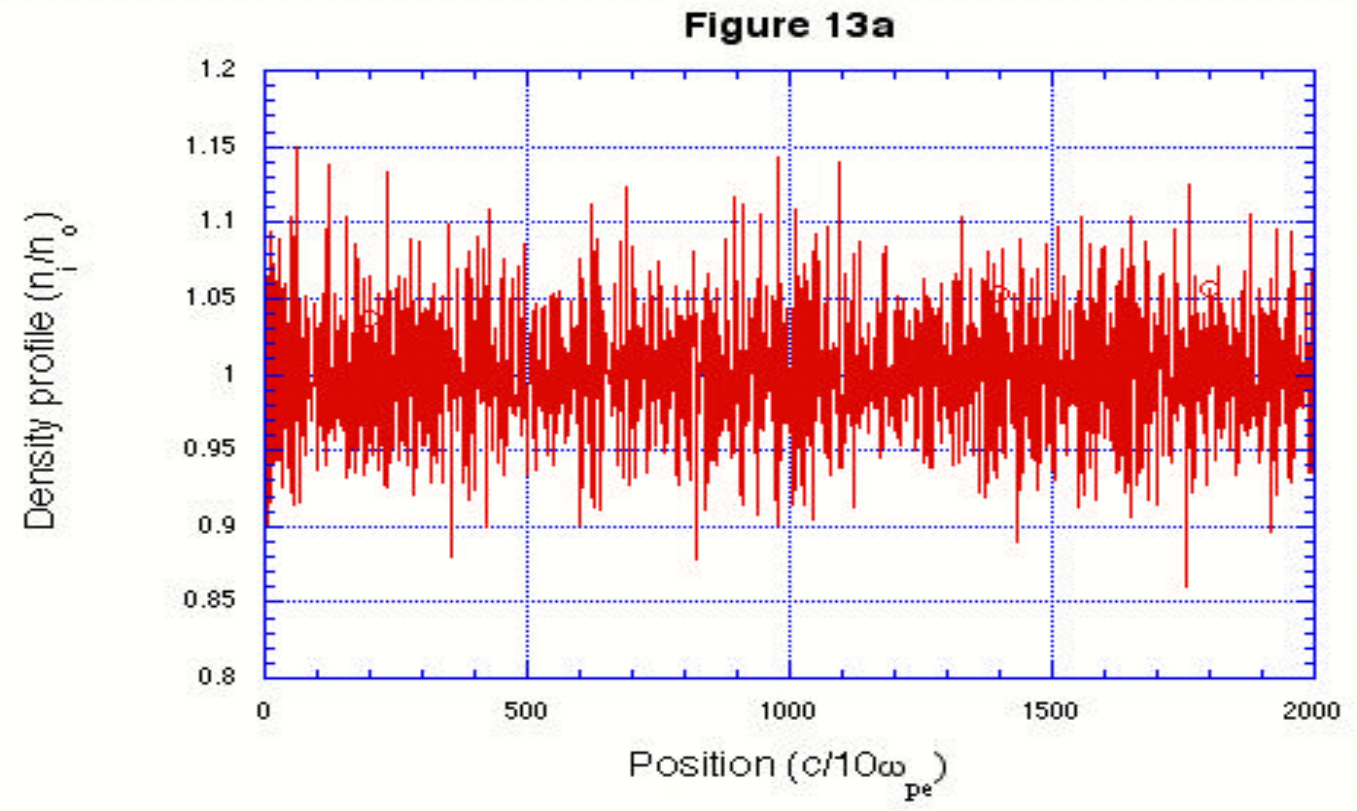

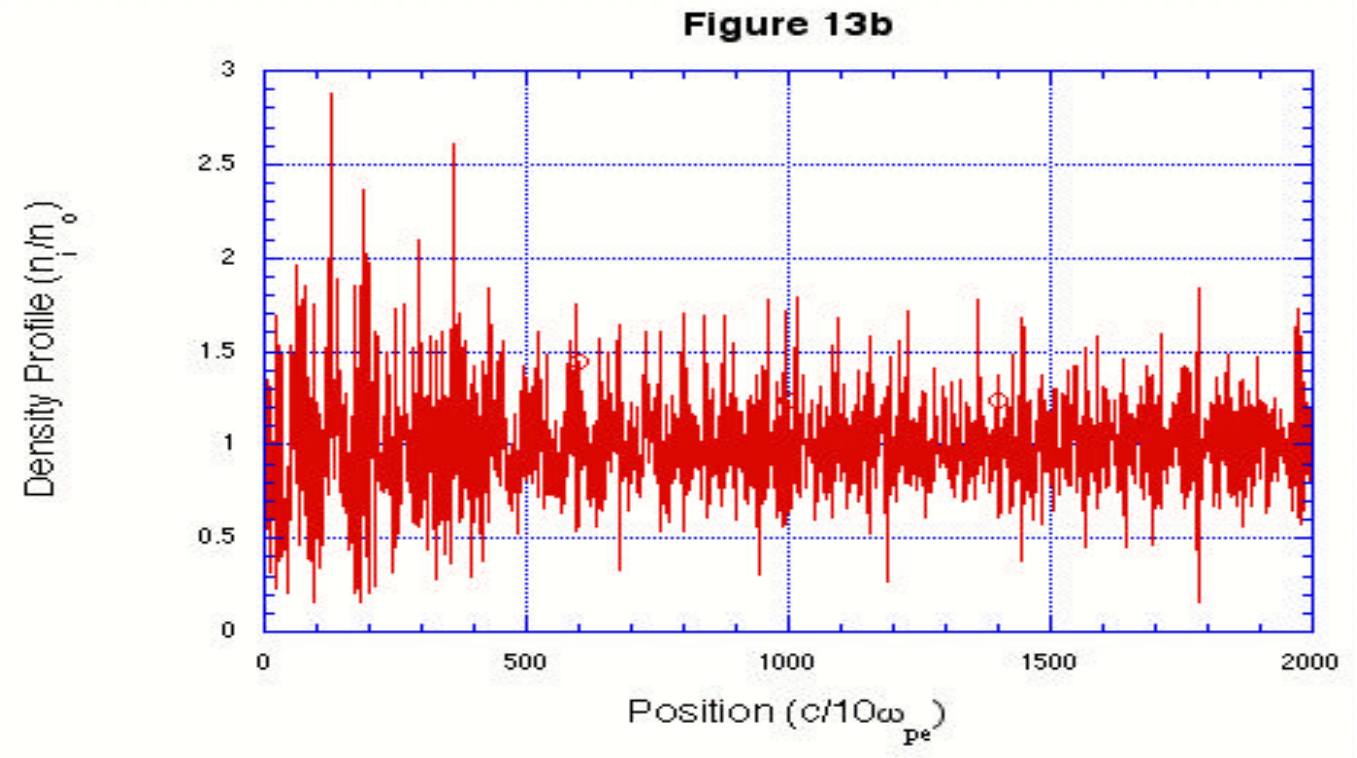

Figure 13. Plasma density fluctuations for 1 keV plasma run (early)

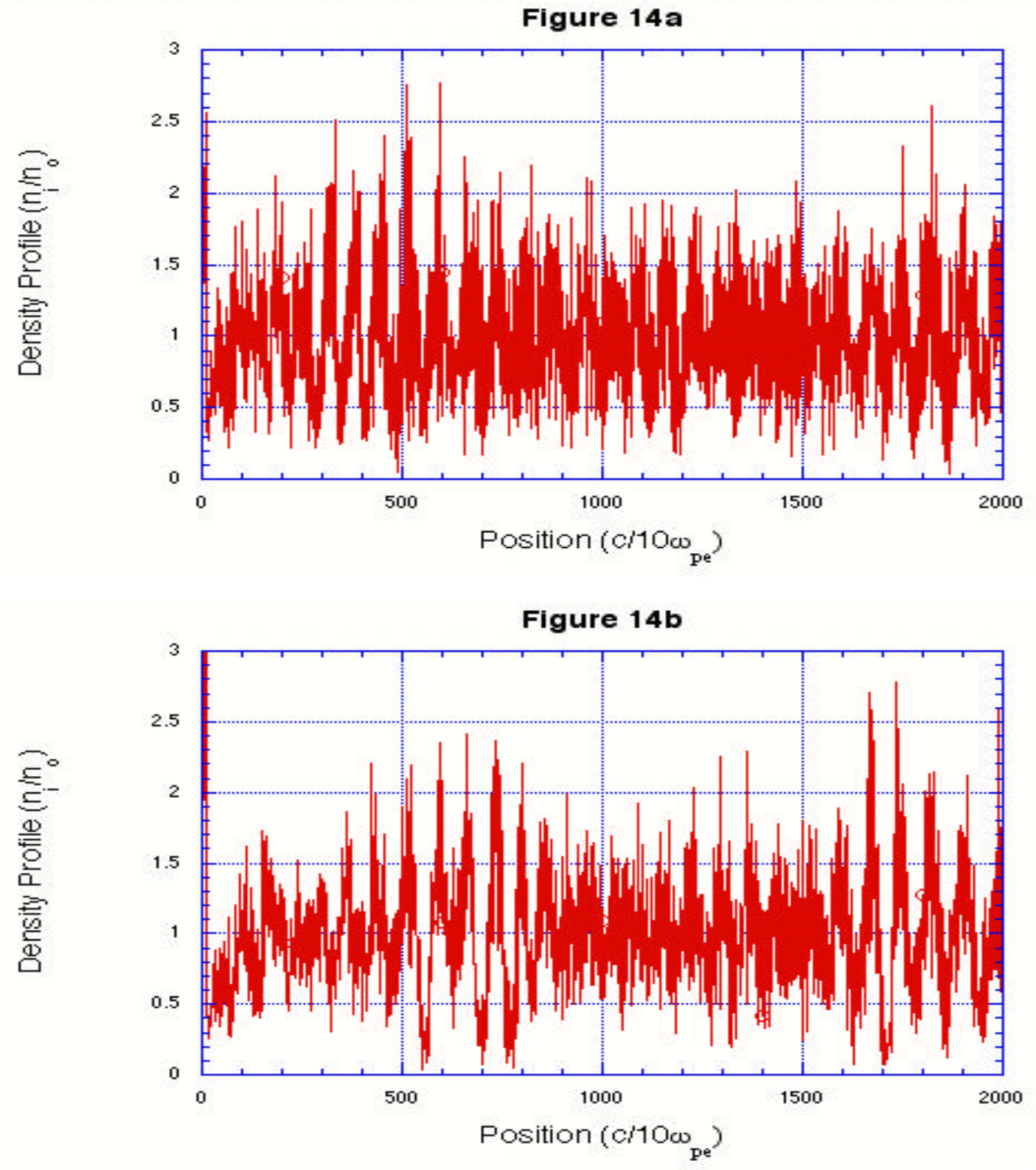

Figure 14. Plasma density fluctuations for 1 keV plasma run (late)

Figure 15. 2. OMEGA Laser Experiments at 15% critical density

Particle in cell codes, such as Turbowave, are flexible tools to explore many possibilities and parameters. Many scientists are using PIC codes to investigate how to limit the creation of hot electrons and Raman scattering. Hot electrons help preheat the fuel, which then prevents the full compression of the fuel to occur. This is a significant problem if you are trying to make laser fusion successful. Others are seeking ways to increase the generation of hot electrons in order to conduct Nuclear Weapons Effects Testing (NWET) experiments. More hot electrons mean that more high-energy x-rays will be created from the bremmstrahlung of the electrons with a high Z material. It would help both camps if we can understand when SRS is efficient and when it is not. Indeed, some recent experiments with the OMEGA laser explored hot electron generation for lower intensities and shorter wavelength laser light (Ref. 13). In these experiments, gasbag plasmas with various densities were irradiated with 0.35μm laser light at an intensity of about 10^{15} W/cm^2. Typically f_{HOT} was measured to be only a few percent.

Some simulations relating to these Omega experiments were carried out using the Turbowave program. Effects such as much reduced absorption into high-energy electrons was readily seen in simulations with lower intensity laser light. However, our simulated plasmas were too small and the hot electron generation too weak to provide reliable comparisons with experiments. PIC simulations are ideal for investigating strongly nonlinear regimes, such as in the AWE experiments at high intensity. It is much harder to accurately compute the hot electron generation when it is weak, especially with simulations on a MAC G4. One would need to use a supercomputer that would enable simulation of very large, weakly driven plasmas over much longer times with many more particles. Details such as density gradients in the experiments would also need to be considered. Such simulations are beyond the scope of this thesis, which is more focused on high intensity experiments where the hot electron generation is strong, as desired for an x-ray source.

C. ANALYSIS OF THE FOURIER TRANSFORMS OF SELECTED RUNS

Another useful tool to analyze the computer simulations is to take a Fourier transform of the transverse electric field near the left-most boundary of plasma. This will show the frequency components that make up the electric field. We will look briefly at the previous example; the .23 n_{cr} run that was conducted with an electron temperature of 2.5 keV.

Figure 15 shows the results for the $n_e = 0.23 n_{cr}$ simulation in which we would expect two peaks, indicating the incident laser light field and the Raman-scattered light. In the figure, spectral density (in relative terms) is plotted against w/w_{pe}. As expected, we see a well-defined peak at approximately $w/w_{pe} = 2.1$, which shows the incident laser light. We also see a range of lower frequencies that shows the Raman-scattered light. If we look closer in Figure 16, we see that the range of frequencies is from about $w/w_{pe} = .95 - 1.09$. This spectrum is much broader than expected based on linear theory. However, such a range of frequencies seem quite reasonable when account is taken of the large density fluctuations present in the final nonlinear state in the plasma. Figure 17 shows the same simulation except ion motion is not allowed. Note the very definitive peaks at 2.1, which indicates the incident light, and at about 1.09, which is the Raman backscattered light. Clearly the ion density fluctuations cause the broadening of the scattered light frequency.

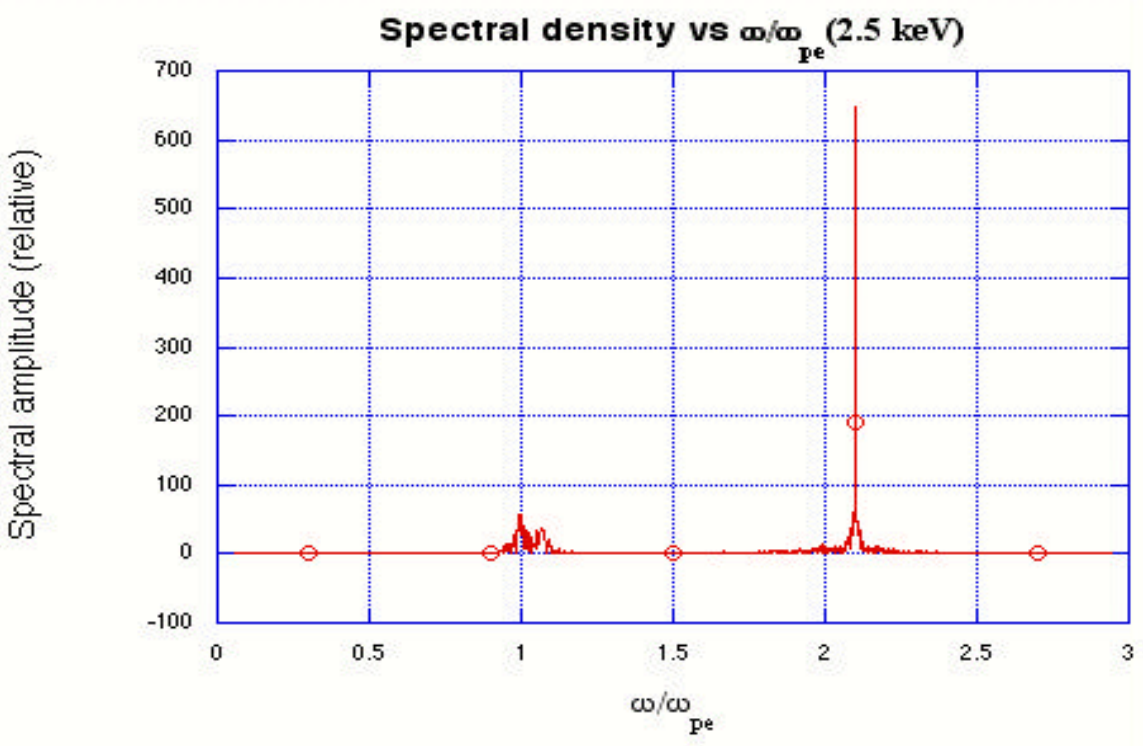

Figure 16. Fourier transform of transverse electric field for 2.5 keV

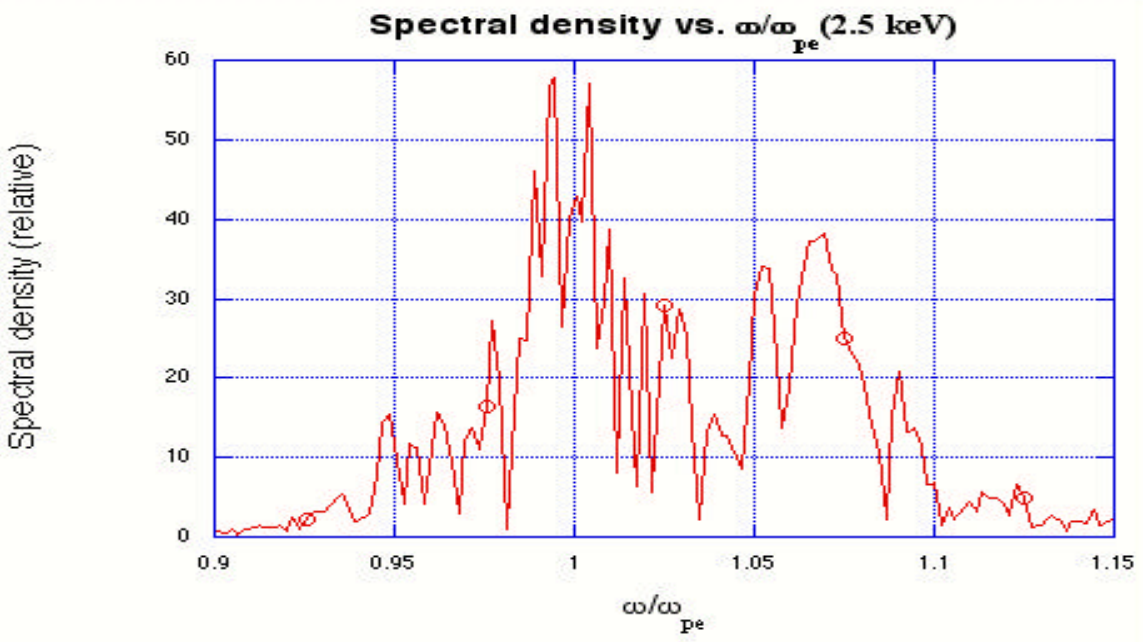

Figure 17. Fourier transform localized showing Raman-scattered frequency

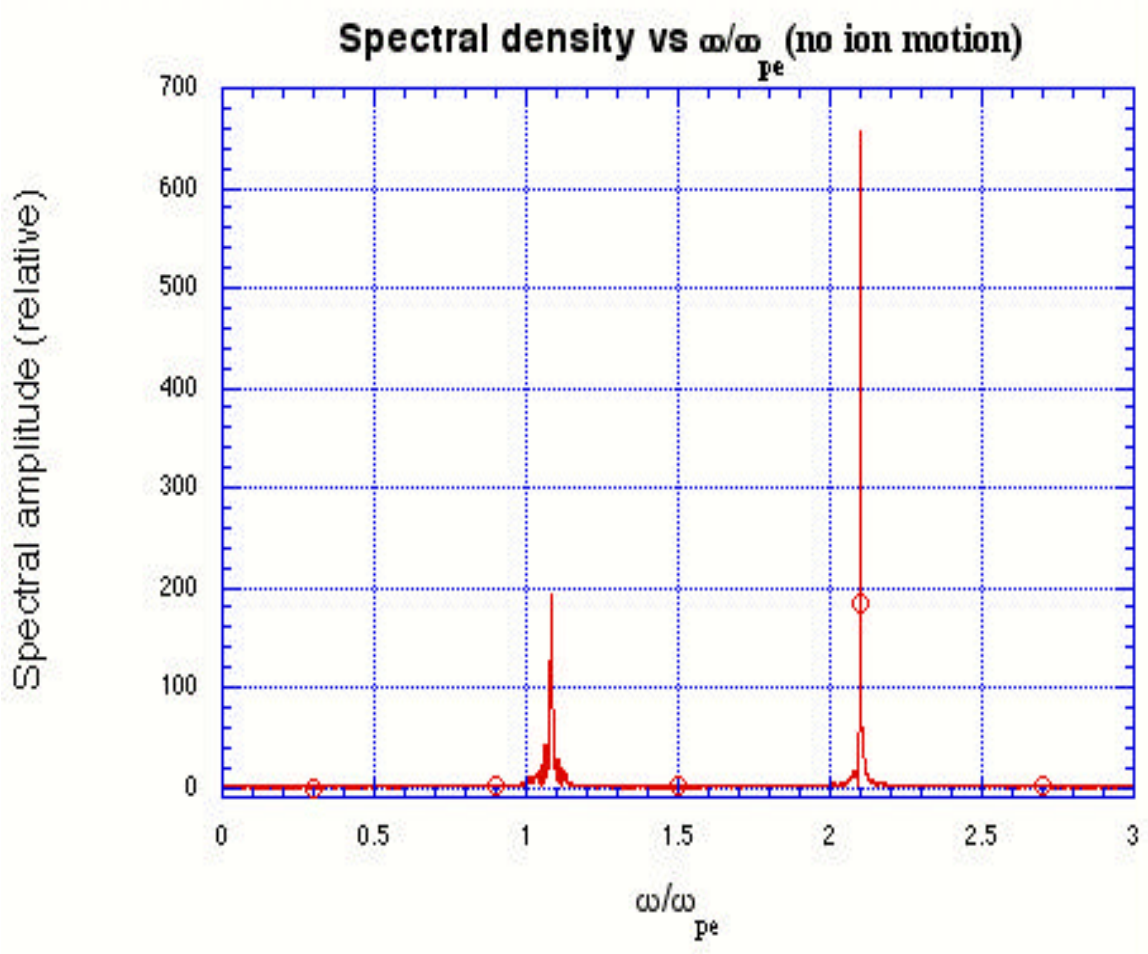

Figure 18. Fourier transform showing frequencies with fixed ions

Figure 19.

Figure 20.

D. SPECTRAL ANALYSIS OF OMEGA SHOTS UTILIZING IDL

Finally, we briefly consider an analysis of some experimental measurements of the scattered light. This data gives the spectrum and intensity of the back-scattered light as a function of time. Such data gives information regarding the density of the plasma from which the scattering is occurring. We use Interactive Data Language (IDL) programming to analyze laser shots conducted by Robert Kirkwood from LLNL in July 2002 on the OMEGA laser at the University of Rochester. Major Mike Ortelli from DOE, Professor Chris Olsen from the Naval Postgraduate School and myself developed the IDL code used. The IDL code takes hierarchal data format (.hdf) files that are produced from the online target diagnostic Full Aperture Backscatter System (FABS) and converts them into portable network graphics (.png) as seen in Figure 18.

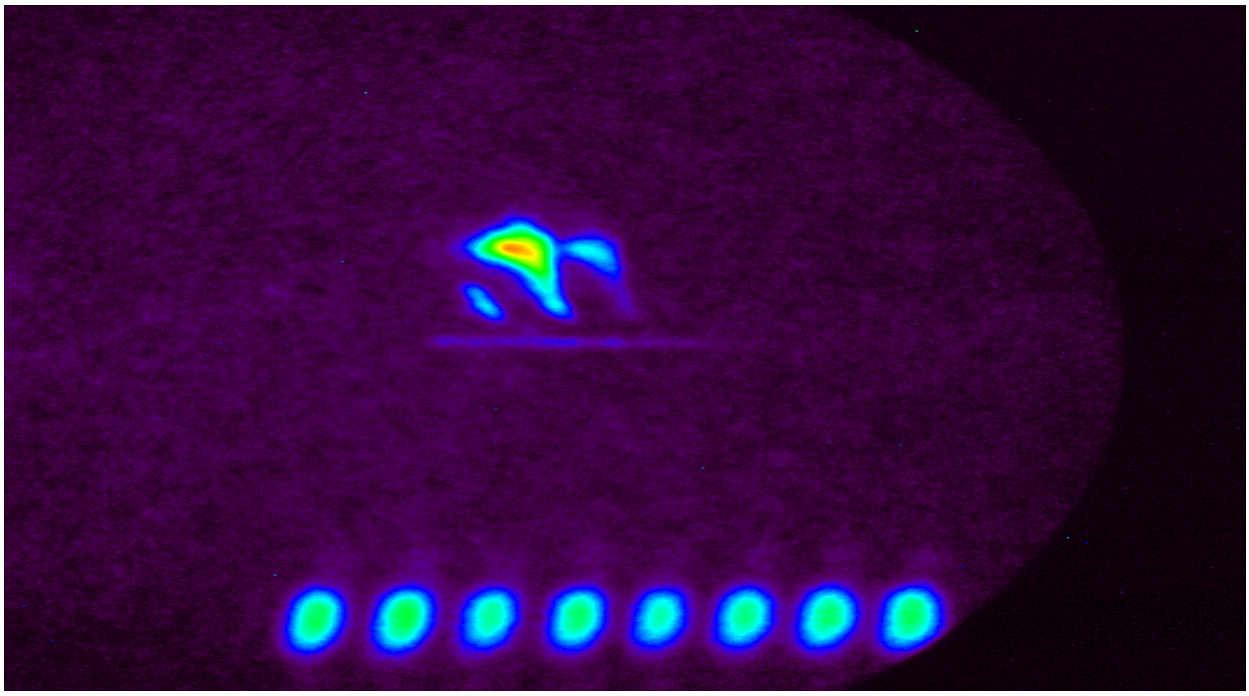

Figure 21. Stimulated Raman Scattered streak in .png format

These graphics clearly show the SRS streak as a function of time, with wavelength increasing with ascension up the y-axis. You can see a characteristic streak at about 532 nm, which shows the incident green laser light from the conversion crystal. You can estimate the time scale by looking at the fiducial at the bottom of the figure. The distance between each of the marker is approximately 1/2 nanosecond. Therefore we

can estimate that the overall length of this laser shot was approximately 1 – 1.5 nanoseconds. Once we have this image, we can do a spectral density image using the IDL program. From this spectral image density we can see the intensity of the scattered light as a function of wavelength and time. This image is not exactly correct, as it does not take into account the dispersion within the fiber optics of the system. Dispersion is caused when different wavelengths of light travel at different speeds within a medium (other than vacuum). In the fiber red light travels faster than blue light and this must be taken into account. Within the IDL program, we incorporated a modified fiber dispersion correction that we received from Wolf Seka (Ref 14), who has conducted similar analysis on other OMEGA experiments. This fiber correction is shown in Figure 19, which shows the shift in time when dispersion is taken into account for wavelengths of less than 550nm. In Figure 20, we can see the spectral density plot after the fiber correction is taken into account. This plot shows a contour map of the relative intensities. If you compare Figures 18 and 20, you can see that plot follows very closely the actual spectral density plot downloaded from OMEGA; however in this case the fiber correction did not make a significant difference. When available, an improved fiber correction can be incorporated for future data analysis. Finally, in Figure 21 we plot the intensity integrated over time as a function of wavelength. In this data, the scattered light peaks at a wavelength of about 650 nm, which corresponds to SRS from a density of about .16 n_{cr}.

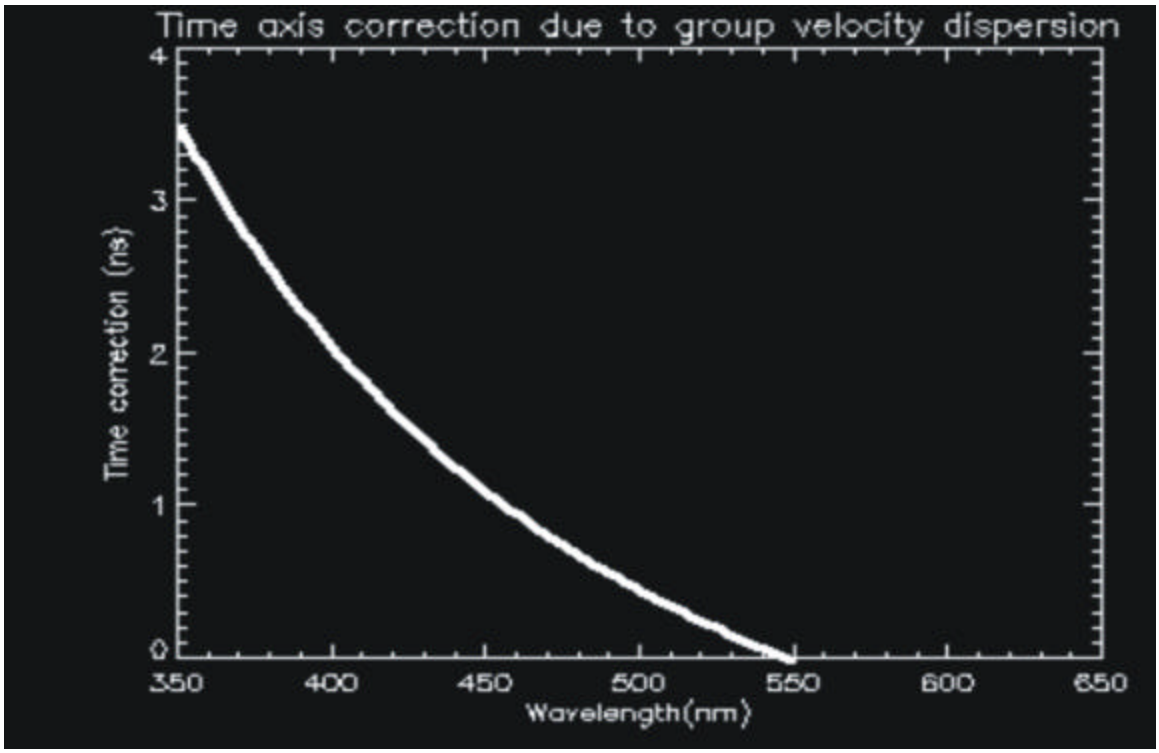

Figure 22. 20m Fiber Correction Graph for OMEGA laser

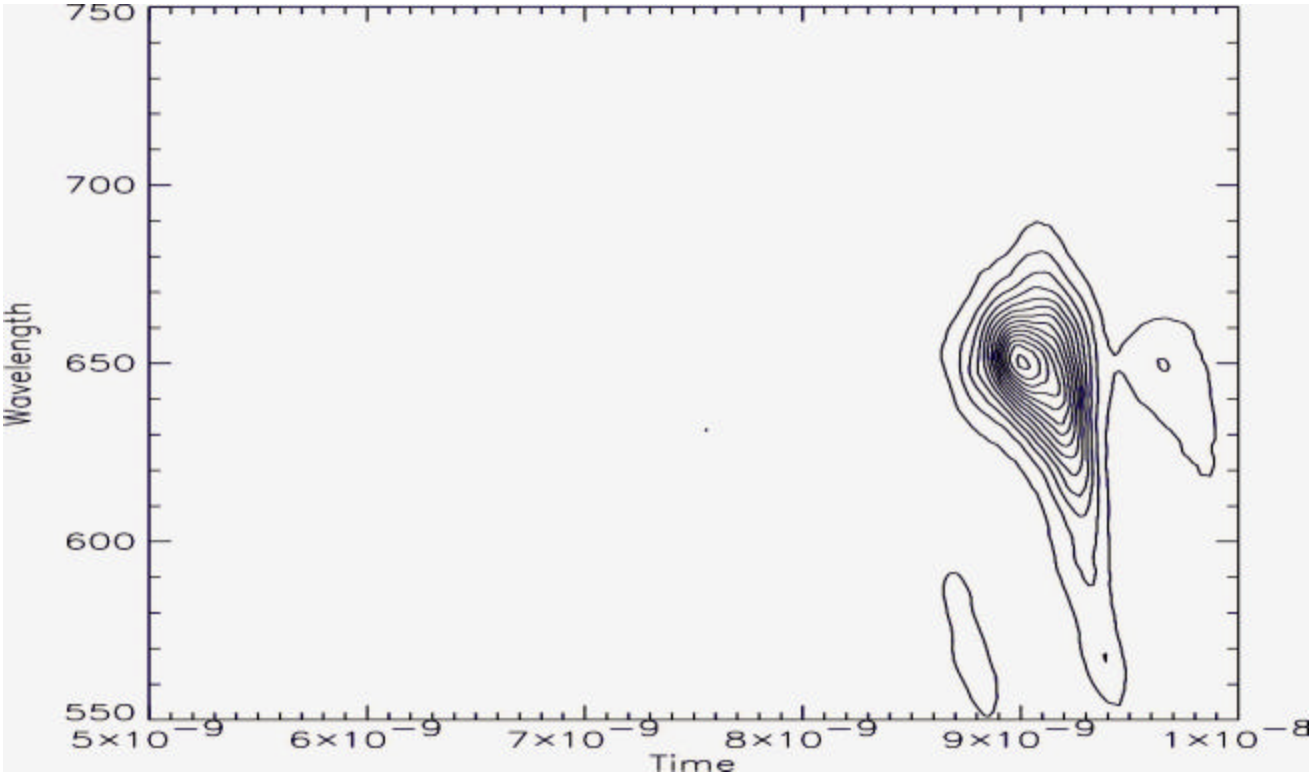

Figure 23. Wavelength (nm) of scattered light vs. Time (ns) profile for OMEGA Shot 20558

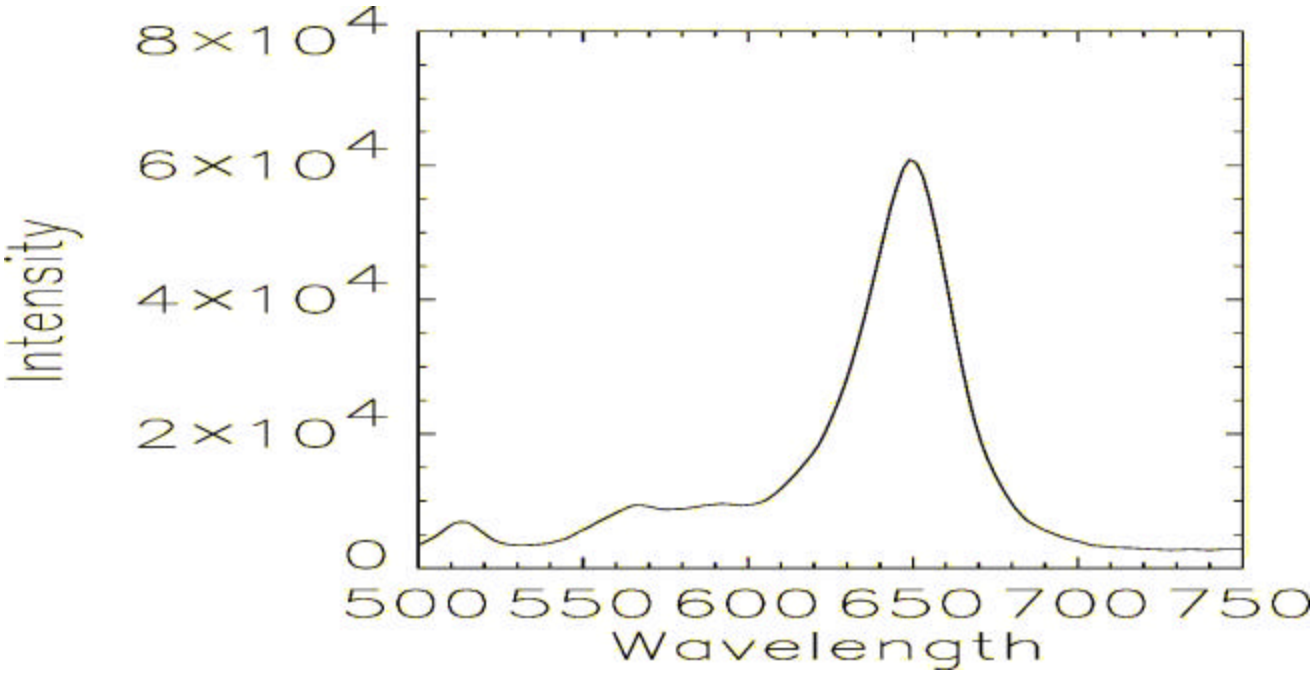

Figure 24. Intensity of scattered light vs. Wavelength integrated over time OMEGA Shot 2055

V. CONCLUSIONS

Stimulated Raman scattering (SRS) represents the resonant decay of an intense light wave into an electron plasma wave plus a scattered light wave. When the electron plasma wave becomes large in amplitude, it accelerates electrons to a high energy. These high energy electrons can be used to produce a high energy x-ray source for NWET. Generation of such a x-ray source is another possible application for the National Ignition Facility.

Computer simulations were used to investigate the high-energy electron generation by SRS. Efficient generation was found when plasma with a density of about 0.25 n_{cr} is irradiated with intense 0.53 μm laser light. The simulations compare favorably with experimental data from the HELEN laser in the United Kingdom. In both experiments and simulations the heated electron temperature was about 30 keV.

The simulations show that the temperature of the heated electrons is strongly reduced and the frequency spectrum of the scattered light is broadened by large ion density fluctuations that form in the plasma. These long wavelength density fluctuations are associated with the ion acoustic wave which forms when the Raman-scattered light waves undergo stimulated Brillouin scattering; i.e. decay into a backscattered light wave plus an ion acoustic wave. In related work, the spectrum of the Raman-scattered light measured in some OMEGA experiments was analyzed using an IDL code.

Finally, the computer simulations also show that the efficiency of high energy electron generation is much reduced when lower intensity, shorter wavelength laser light is used. This trend agrees with some experiments with the OMEGA laser, where the absorption into hot electrons was observed to be only a few percent. Realistic simulation of this weak regime would require use of super computers, which could be a future thesis topic.

THIS PAGE INTENTIONALLY LEFT BLANK

LIST OF REFERENCES

1. Lindl, John D., Inertial Confinement Fusion, (Springer-Verlag), New York, NY 1998
2. Jones, W. David.,"Advanced Applications for 0.53 μm Laser Light", Thesis, Naval Postgraduate School, June 2001
3. Ortelli, Michael A., "Energetic Electron Generation by Forward Stimulated Raman Scattering using 0.35 and 0.53 Micron Laser Light in a Plasma", Thesis, Naval Postgraduate School, June 2001
4. Kruer, William L., Physics of Laser Plasma Interactions, (Addison-Wesley), Redwood City, 1988
5. Kruer, W.L.,Campbell, E.M., Deckert, C.D., Wilks, S.C., Moody, J., Orzechowski, T., Powers, L., Suter, L.J., Afeyan, B.B., and Dague, N., Plasma Phys. Control Fusion 41, A409 (1999)
6. Chen, Francis F., Introduction to Plasma Physics and Controlled Fusion Vol I, (Plenum Press), New York, NY 1984
7. Campbell, E.M., Eimerl, D, Kruer, W.L.,Weber, S and Verdon, C.P., Comments Plasma Phys. Controller Fusion 18, 201 (1997)
8. Estabrook, Kent and Kruer, W.L., Phys. Fluids 26, 1892 (1983)
9. Langdon, A.B., Lasinski, B.F. and Kruer, W.L., Phys. Rev. Letters 43, 133 (1979)
10. Birdsall, C.K. and Langdon, A.B., Plasma Physics via Computer Simulation, Institute of Physics Publishing, Philadelphia, PA 1998
11. Gordon, D., Mori, W.B., and Antonsen Jr, Tom., IEEE Trans. Plasma Sci. 28, 1224 (2000)
12. Suter, L., Miller, M., Back, C., Kruer, W., Stevenson, M., Oades, K., Slark, G., Foster, J., Grun, J. and Davis, J., Green Light Interaction Experiments on HELEN, WBS-1 Review (February 7-8, 2002)
13. Miller, M.C., Kirkwood, R.K., Suter, L.J., Glenzer, S.H., Back, C.A., Stoeckl, C., Wallace, R.J., Hsing, W.W., Kruer, W.L., and Ortelli, M., Suprathermal Radiation Source Experiments on OMEGA, APS-DPP Meeting (October 26, 2000)
14. Wolf Seka, private communication, 2002

THIS PAGE INTENTIONALLY LEFT BLANK

INITIAL DISTRIBUTION LIST

1. Defense Technical Information Center
   Ft. Belvoir, VA

2. Dudley Knox Library
   Naval Postgraduate School
   Monterey, CA

3. Engineering and Technology Curricular Office, Code 34
   Naval Postgraduate School
   Monterey, CA

4. Professor William L. Kruer, Code PH/Kw
   Naval Postgraduate School
   Monterey, CA

5. Professor William B. Colson, Code PH/Cw
   Naval Postgraduate School
   Monterey, CA

6. Defense Threat Reduction Agency (DTRA)
   Ft. Belvoir, VA

7. LT. Martin Wallace
   FPO AP

8. Physics Department
   Naval Postgraduate School
   Monterey, CA